

A POSTERIORI ERROR ESTIMATES FOR FINITE ELEMENT DISCRETIZATIONS OF TIME-HARMONIC MAXWELL'S EQUATIONS COUPLED WITH A NON-LOCAL HYDRODYNAMIC DRUDE MODEL

T. CHAUMONT-FRELET^{†,‡}, S. LANTERI^{†,‡}, AND P. VEGA[†]

ABSTRACT. We consider finite element discretizations of Maxwell's equations coupled with a non-local hydrodynamic Drude model that accurately accounts for electron motions in metallic nanostructures. Specifically, we focus on *a posteriori* error estimation and mesh adaptivity, which is of particular interest since the electromagnetic field usually exhibits strongly localized features near the interface between metals and their surrounding media. We propose a novel residual-based error estimator that is shown to be reliable and efficient. We also present a set of numerical examples where the estimator drives a mesh adaptive process. These examples highlight the quality of the proposed estimator, and the potential computational savings offered by mesh adaptivity.

KEY WORDS. A posteriori error estimates; Finite element methods; Maxwell's equations; Non-local hydrodynamic Drude model; Plasmonics

1. INTRODUCTION

The interaction of light with metallic nanostructures gives rise to so-called plasmonic waves that are due to collective oscillations of conduction band electrons in the metal, and typically concentrate at the interface between the nanostructure and the surrounding medium. These unusual properties allow an extraordinary level of light manipulation at the nanoscale [17], with applications in waveguiding [21], lasing [23], near-field scanning microscopy [20], ultrasensitive sensing [24] and energy harvesting [5].

Electromagnetic fields penetrate in noble metals up to 25 nm whatever the wavelength. Small metallic nanostructures actually contains a plasma, whose electromagnetic response is in opposition to the incoming field, generating plasmonic waves. While this effect is negligible when considering large structures, metals cannot be considered to be perfectly conducting at the nanoscale, and valence electrons have to be modeled as a gas [17], leading to dispersive material laws.

In this work, we focus on the time-harmonic setting where the electromagnetic field oscillates in time at a prescribed frequency $\omega > 0$. In this context, the Drude model [9] is a fairly simple yet efficient oscillator model for free electrons in metals. Standard Maxwell's equations are employed in the metal to describe the propagation of the electric field \mathbf{E} ,

$$(1.1) \quad -\omega^2 \varepsilon_d \mathbf{E} + \nabla \times (\mu_0^{-1} \nabla \times \mathbf{E}) = \mathbf{o}$$

but the permittivity

$$\varepsilon_d := \left(1 - \frac{\omega_p^2}{i\gamma\omega + \omega^2} \right) \varepsilon_0$$

[†]Inria, 2004 Route des Lucioles, 06902 Valbonne, France

[‡]Laboratoire J.A. Dieudonné, Parc Valrose, 28 Avenue Valrose, 06108 Nice Cedex 02, 06000 Nice, France

becomes a complex-valued function of the frequency, with a negative real part at optical frequencies. Above, ε_0 and μ_0 respectively denote the vacuum electric permittivity and magnetic permeability. ω_P and γ are the so-called “plasma” and “collision” frequencies of the metal under consideration. Although the Drude model performs well in most cases, it becomes inaccurate when the size of the considered nanostructure decreases beyond approximately 10 nm. Then, a possible extension is the so-called non-local hydrodynamic Drude (NHD) model [22], where the electron gas is treated as a fluid. Compared to the “local” Drude model for free electrons, this hydrodynamic approach accounts for the Fermi velocity v_F of the electrons via an additional parameter $\beta^2 := (3/5)v_F^2$, namely

$$(1.2) \quad \begin{cases} -\omega^2 \varepsilon_0 \mathbf{E} + \nabla \times (\mu_0^{-1} \nabla \times \mathbf{E}) + i\omega \mathbf{J} &= \mathbf{o}, \\ -\omega^2 \mathbf{J} - i\omega \gamma \mathbf{J} - \nabla (\beta^2 \nabla \cdot \mathbf{J}) - i\omega \omega_P^2 \varepsilon_0 \mathbf{E} &= \mathbf{o}, \end{cases}$$

where the motion of the electrons is now explicitly modeled through the velocity field \mathbf{J} . Notice that setting $\beta := 0$, (1.2) reduces to (1.1). Thanks to its relatively simple form and the successful interpretation of observable non-local effects [10], the NHD model has become a quite popular approach in the study of optical properties of metallic nanostructures.

The above considerations have naturally led to an increasing interest for efficient numerical discretizations of Maxwell’s equations coupled with NHD model (1.2) in metallic nanostructures. Several approaches have been considered, including boundary integral equations [28], discontinuous Galerkin schemes [15, 27] and finite element methods [14, 16, 25]. Here, we focus on finite element discretizations, which have the advantage to easily handle heterogeneous media as compared to integral equations, while being simpler to implement and analyze than discontinuous Galerkin schemes. The ability to work on unstructured meshes not only permits to deal with arbitrary geometries, but it also allows for local mesh refinements. Such local refinements increase the accuracy in those areas where the solution exhibit a complex behavior at a reduced cost, and seem of particular interest in the context of nanoplasmonics, since plasmons are in general strongly localized. Here, we thus focus on the design and analysis of *a posteriori* error estimators, and their ability to drive mesh adaptive algorithms [2, 26].

Our main contributions are threefold. First, we propose a novel *a posteriori* error estimator for finite element discretizations of the Maxwell-NHD system in general three-dimensional configurations. Our estimator is of “residual” type, and builds upon previous constructions for standard Maxwell’s equations [4, 6, 19] with suitable modifications to handle the NHD model. Our second key contribution is a detailed mathematical analysis of the estimator, where we show that it is both reliable and efficient in a suitable energy norm. Finally, we numerically evaluate the ability of the estimator to drive adaptive processes, and quantify the computational savings as compared to uniform meshes. To this end, we consider three two-dimensional examples that are representative of typical nanoplasmonic applications. In each case, the use of adaptivity leads to a drastic reduction of the number of required degrees of freedom to achieve any given accuracy. These preliminary results are very promising in view of more realistic three-dimensional applications.

To the best of our knowledge, most existing studies on the NHD model focus on the development of numerical methods or the analysis of physical effects. In comparison, the rigorous mathematical analysis is relatively recent, and *a priori* error estimates have been only recently established [16]. As a result, the proposed analysis appears to be entirely original.

The remainder of this manuscript is organized as follows. In Section 2, we present our model problem, notations and preliminary results. Section 3 introduces the *a posteriori* error estimator and establishes our main theoretical results. We provide numerical examples in Section 4 and draw our conclusions in Section 5.

2. SETTINGS

2.1. Maxwell-NHD equations. In this work, $\Omega \subset \mathbb{R}^3$ is a polyhedral Lipschitz domain, and $\Omega_m \subset\subset \Omega$ is a Lipschitz polyhedral subset. Ω_m can be multi-connected, but the boundaries of Ω and Ω_m are not allowed to touch each other. Whenever convenient, we will implicitly extend scalar-valued (resp. vector-valued) functions defined in Ω_m by 0 (resp. \mathbf{o}) in $\Omega \setminus \Omega_m$.

For the sake of simplicity, we consider a generalization of (1.2) with more general coefficients that we now describe. We assume that Ω is subdivided into a polyhedral partition \mathcal{P} that is conforming with Ω_m in the sense that any subset $P \in \mathcal{P}$ either entirely belongs to $\overline{\Omega}$ or $\overline{\Omega_m}$. Then $\varepsilon, \chi : \Omega \rightarrow \mathcal{L}(\mathbb{C}^3)$, $\alpha : \Omega_m \rightarrow \mathcal{L}(\mathbb{C}^3)$ and $\zeta : \Omega_m \rightarrow \mathbb{C}$ are assumed to be piecewise constant onto \mathcal{P} .

We do not require the tensor-valued functions neither to be symmetric, nor to be positive-definite. Also, ζ is allowed to change sign. The only assumption we require is that the problem is inf-sup stable (see Assumption 2.1 below) which implicitly constrains the coefficients.

For $\mathbf{x} \in \Omega$, we denote by

$$\varepsilon^*(\mathbf{x}) := \max_{\substack{\mathbf{u} \in \mathbb{C}^3 \\ |\mathbf{u}|=1}} \max_{\substack{\mathbf{v} \in \mathbb{C}^3 \\ |\mathbf{v}|=1}} \operatorname{Re}(\varepsilon(\mathbf{x})\mathbf{u} \cdot \bar{\mathbf{v}}), \quad \chi^*(\mathbf{x}) := \max_{\substack{\mathbf{u} \in \mathbb{C}^3 \\ |\mathbf{u}|=1}} \max_{\substack{\mathbf{v} \in \mathbb{C}^3 \\ |\mathbf{v}|=1}} \operatorname{Re}(\chi(\mathbf{x})\mathbf{u} \cdot \bar{\mathbf{v}})$$

and similarly, for $\mathbf{x} \in \Omega_m$, we write

$$\alpha^*(\mathbf{x}) := \max_{\substack{\mathbf{u} \in \mathbb{C}^3 \\ |\mathbf{u}|=1}} \max_{\substack{\mathbf{v} \in \mathbb{C}^3 \\ |\mathbf{v}|=1}} \operatorname{Re}(\alpha(\mathbf{x})\mathbf{u} \cdot \bar{\mathbf{v}}), \quad \zeta^*(\mathbf{x}) := |\zeta(\mathbf{x})|.$$

For the sake of simplicity, we implicitly extend α^* and ζ^* by zero in $\Omega \setminus \overline{\Omega_m}$. If $\phi \in \{\varepsilon, \chi, \alpha, \zeta\}$, we introduce the notations $\phi_K^* := \phi^*|_K \in \mathbb{R}$ as well as

$$\phi_{D,\min} := \operatorname{ess\,inf}_{\mathbf{x} \in D} \phi^*(\mathbf{x}), \quad \phi_{D,\max} := \operatorname{ess\,sup}_{\mathbf{x} \in D} \phi^*(\mathbf{x})$$

for any open set $D \subset \Omega$, and we assume that $\varepsilon_{\Omega,\min}, \mu_{\Omega,\min}, \alpha_{\Omega_m,\min}, \zeta_{\Omega_m,\min} > 0$.

We are now ready to state our model problem. Namely, given $\mathbf{J}_e : \Omega \rightarrow \mathbb{C}^3$ and $\mathbf{K}_e : \Omega_m \rightarrow \mathbb{C}^3$, we seek $\mathbf{E} : \Omega \rightarrow \mathbb{C}^3$ and $\mathbf{J} : \Omega_m \rightarrow \mathbb{C}^3$ such that

$$(2.1) \quad \begin{cases} -\omega^2 \varepsilon \mathbf{E} + \nabla \times (\chi \nabla \times \mathbf{E}) + i\omega \mathbf{J} & = i\omega \mathbf{J}_e & \text{in } \Omega, \\ -\omega^2 \alpha \mathbf{J} - \nabla (\zeta \nabla \cdot \mathbf{J}) - i\omega \mathbf{E} & = i\omega \mathbf{K}_e & \text{in } \Omega_m. \end{cases}$$

On the one hand, we recover (1.2) when

$$\varepsilon := \varepsilon_0 \mathbf{I}, \quad \chi := \mu_0^{-1} \mathbf{I}, \quad \alpha := \frac{1}{\omega_p^2 \varepsilon_0} \left(1 - \frac{1}{i\omega} \gamma \right) \mathbf{I}, \quad \zeta := \frac{\beta^2}{\omega_p^2 \varepsilon_0}.$$

On the other hand, the proposed reformulation permits to treat more general cases in a uniform manner, without adding any mathematical complexity. In particular, the permittivity is allowed to change sign, which enables to take into account the local Drude model. Besides, our analysis naturally handles anisotropic materials, and in particular, perfectly matched layers can be employed to model unbounded propagation media [18].

For later use, we notice that as usual in the analysis of Maxwell's equations, there are two "hidden" equations in (2.1), namely

$$(2.2) \quad \nabla \cdot (i\omega\varepsilon\mathbf{E} + \mathbf{J}) = \nabla \cdot \mathbf{J}_e \text{ in } \Omega$$

and

$$(2.3) \quad \nabla \times (i\omega\alpha\mathbf{J} - \mathbf{E}) = \nabla \times \mathbf{K}_e \text{ in } \Omega_m.$$

We also notice that there are three different (space-dependent) wavenumbers appearing in the above model. As usual, the electromagnetic wavenumber is defined in Ω by

$$(2.4a) \quad k_E := \frac{\omega}{c_E}, \quad c_E := \sqrt{\frac{\chi^*}{\varepsilon^*}},$$

and in addition, we introduce

$$(2.4b) \quad k_J := \frac{\omega}{c_J}, \quad k_P := \frac{\omega_P}{c_P}, \quad c_J := \sqrt{\frac{\zeta^*}{\alpha^*}}, \quad c_P := \omega_P \sqrt{\zeta^* \varepsilon^*},$$

in Ω_m . We add, for all the notations in (2.4), a second subscript K for the (constant) restrictions to $K \in \mathcal{T}_h$.

2.2. Functional spaces. If $D \subset \Omega$ is an open set, $L^2(D)$ denotes the space of complex-valued square-integrable functions defined on D , and $\mathbf{L}^2(D) := (L^2(D))^3$. The notations $\|\cdot\|_D$ and $(\cdot, \cdot)_D$ stand for the usual norm and inner-product of $L^2(D)$ and $\mathbf{L}^2(D)$. For $\phi \in \{\varepsilon, \chi, \alpha, \zeta\}$, we introduce the (equivalent) norms on $L^2(D)$ and $\mathbf{L}^2(D)$ defined by

$$\|w\|_{\phi, D}^2 := \int_D \phi^* |w|^2, \quad \|\mathbf{w}\|_{\phi, D}^2 := \int_D \phi^* |\mathbf{w}|^2,$$

$w \in L^2(D)$ and $\mathbf{w} \in \mathbf{L}^2(D)$.

$H^1(D)$ is the usual first-order Sobolev space of functions $v \in L^2(D)$ such that $\nabla v \in \mathbf{L}^2(D)$. If $\Gamma \subset \partial\Omega$ is a relatively open set, $H_\Gamma^1(D)$ stands for the space of functions $v \in H^1(D)$ such that $v|_\Gamma = 0$. For vector-valued functions, we also introduce $\mathbf{H}^1(D) := (H^1(D))^3$ and $\mathbf{H}_\Gamma^1(D) := (H_\Gamma^1(D))^3$.

We will also need the vector Sobolev spaces

$$\begin{aligned} \mathbf{H}(\mathbf{curl}, D) &:= \{\mathbf{v} \in \mathbf{L}^2(D) \mid \nabla \times \mathbf{v} \in \mathbf{L}^2(D)\}, \\ \mathbf{H}(\text{div}, D) &:= \{\mathbf{v} \in \mathbf{L}^2(D) \mid \nabla \cdot \mathbf{v} \in L^2(D)\}, \end{aligned}$$

and there subspaces $\mathbf{H}_0(\mathbf{curl}, D)$ and $\mathbf{H}_0(\text{div}, D)$ that are defined, as usual, as the closure of smooth compactly supported functions.

The aforementioned functional spaces are widely documented in the literature, and we refer the reader to [1, 12] for a precise description.

We finally introduce the "energy" space

$$\mathbb{V} := \mathbf{H}_0(\mathbf{curl}, \Omega) \times \mathbf{H}_0(\text{div}, \Omega_m),$$

that we equip with the norm

$$\|(\mathbf{e}, \mathbf{j})\|^2 := \omega^2 \|e\|_{\varepsilon, \Omega}^2 + \|\nabla \times e\|_{\chi, \Omega}^2 + \omega^2 \|\mathbf{j}\|_{\alpha, \Omega_m}^2 + \|\nabla \cdot \mathbf{j}\|_{\zeta, \Omega_m}^2, \quad (\mathbf{e}, \mathbf{j}) \in \mathbb{V}.$$

If $D \subset \Omega$ is an open set, we will also use the local version

$$\|(\mathbf{e}, \mathbf{j})\|_D^2 := \omega^2 \|e\|_{\varepsilon, D}^2 + \|\nabla \times e\|_{\chi, D}^2 + \omega^2 \|\mathbf{j}\|_{\alpha, D \cap \Omega_m}^2 + \|\nabla \cdot \mathbf{j}\|_{\zeta, D \cap \Omega_m}^2, \quad (\mathbf{e}, \mathbf{j}) \in \mathbb{V}.$$

2.3. Well-posedness. We denote by $b : \mathbb{V} \times \mathbb{V} \rightarrow \mathbb{C}$ the sesquilinear form naturally associated with (2.1) after integration by parts. It is defined by

$$b((\mathbf{e}, \mathbf{j}), (\mathbf{v}, \mathbf{w})) := -\omega^2(\boldsymbol{\varepsilon}\mathbf{e}, \mathbf{v})_\Omega + (\boldsymbol{\chi}\boldsymbol{\nabla} \times \mathbf{e}, \boldsymbol{\nabla} \times \mathbf{v})_\Omega + i\omega(\mathbf{j}, \mathbf{v})_{\Omega_m} \\ - \omega^2(\boldsymbol{\alpha}\mathbf{j}, \mathbf{w})_{\Omega_m} + (\boldsymbol{\zeta}\boldsymbol{\nabla} \cdot \mathbf{j}, \boldsymbol{\nabla} \cdot \mathbf{w})_{\Omega_m} - i\omega(\mathbf{e}, \mathbf{w})_{\Omega_m}$$

for all $(\mathbf{e}, \mathbf{j}), (\mathbf{v}, \mathbf{w}) \in \mathbb{V}$. Then, a weak formulation of (2.1) consists in finding $(\mathbf{E}, \mathbf{J}) \in \mathbb{V}$ such that

$$(2.5) \quad b((\mathbf{E}, \mathbf{J}), (\mathbf{v}, \mathbf{w})) = i\omega(\mathbf{J}_e, \mathbf{v}) + i\omega(\mathbf{K}_e, \mathbf{w}) \quad \forall (\mathbf{v}, \mathbf{w}) \in \mathbb{V}.$$

In the remaining of this work, we require that the sesquilinear form b is inf-sup stable, which implies well-posedness of (2.5). Specifically, we make the following assumption.

Assumption 2.1 (Well-posedness). *There exists a constant $\mathcal{C}_{i/s}$ such that*

$$(2.6) \quad \inf_{(\mathbf{e}, \mathbf{j}) \in \mathbb{V} \setminus \{0\}} \sup_{(\mathbf{v}, \mathbf{w}) \in \mathbb{V} \setminus \{0\}} \frac{\operatorname{Re} b((\mathbf{e}, \mathbf{j}), (\mathbf{v}, \mathbf{w}))}{\|(\mathbf{e}, \mathbf{j})\| \|(\mathbf{v}, \mathbf{w})\|} \geq \mathcal{C}_{i/s} > 0.$$

2.4. Mesh. We consider a mesh \mathcal{T}_h of Ω made of tetrahedral elements K . \mathcal{T}_h is conforming in the sense of [7], which means that the intersection $\overline{K_-} \cap \overline{K_+}$ of two distinct elements $K_\pm \in \mathcal{T}_h$ is either empty, or a single vertex, edge or face of both elements. We further assume that \mathcal{T}_h is conforming with \mathcal{P} , in the sense for each $K \in \mathcal{T}_h$, there exists $P \in \mathcal{P}$ such that $\overline{K} \subset \overline{P}$. We denote by $\mathcal{T}_{m,h}$ the restriction of \mathcal{T}_h to Ω_m , i.e., the set of those $K \in \mathcal{T}_h$ such that $\overline{K} \subset \overline{\Omega_m}$.

Following [7], we employ the notations

$$h_K := \max_{\mathbf{x}, \mathbf{y} \in \overline{K}} |\mathbf{x} - \mathbf{y}|, \quad \rho_K := \max \{r > 0 \mid \exists \mathbf{x} \in \overline{K}; B(\mathbf{x}, r) \subset \overline{K}\}$$

for the diameter and inscribed sphere radius of the element $K \in \mathcal{T}_h$. $\kappa_K := h_K/\rho_K$ is then called the shape-regularity parameter of K , and $\kappa := \max_{K \in \mathcal{T}_h} \kappa_K$ is the shape-regularity parameter of \mathcal{T}_h .

We introduce, for $K \in \mathcal{T}_h$ and $F \in \mathcal{F}_h$, the sets

$$\mathcal{T}_{K,h} := \{K' \in \mathcal{T}_h \mid \overline{K} \cap \overline{K'} \neq \emptyset\}, \quad \mathcal{T}_{F,h} := \{K' \in \mathcal{T}_h \mid F \subset \partial K'\},$$

and the associated open domains

$$\tilde{K} := \operatorname{Int} \left(\bigcup_{K' \in \mathcal{T}_{K,h}} \overline{K'} \right), \quad \tilde{F} := \operatorname{Int} \left(\bigcup_{K' \in \mathcal{T}_{F,h}} \overline{K'} \right).$$

When $K \in \mathcal{T}_{m,h}$ and $F \in \mathcal{F}_{m,h}$, we will also use the submeshes $\mathcal{T}_{m,K,h} := \mathcal{T}_{K,h} \cap \mathcal{T}_{m,h}$ and $\mathcal{T}_{m,F,h} := \mathcal{T}_{F,h} \cap \mathcal{T}_{m,h}$, and the associated open domains \tilde{K}_m and \tilde{F}_m .

For $\mathcal{T} \subset \mathcal{T}_h$ and $\mathcal{F} \subset \mathcal{F}_h$, we write

$$\langle \cdot, \cdot \rangle_{\mathcal{T}} := \sum_{K \in \mathcal{T}} \langle \cdot, \cdot \rangle_K, \quad \langle \cdot, \cdot \rangle_{\partial \mathcal{T}} := \sum_{K \in \mathcal{T}} \langle \cdot, \cdot \rangle_{\partial K}, \quad \langle \cdot, \cdot \rangle_{\mathcal{F}} := \sum_{F \in \mathcal{F}} \langle \cdot, \cdot \rangle_F$$

and

$$\mathbf{H}^1(\mathcal{T}) := \{ \mathbf{v} \in \mathbf{L}^2(U) \mid \mathbf{v}|_K \in \mathbf{H}^1(K) \quad \forall K \in \mathcal{T} \},$$

with $U := \operatorname{Int}(\cup_{K \in \mathcal{T}} \overline{K})$.

2.5. Finite element spaces. The usual Lagrange and Nédélec spaces on \mathcal{T}_h read

$$V_h := \mathcal{P}_{p+1}(\mathcal{T}_h) \cap H_0^1(\Omega), \quad \mathbf{W}_h := \mathcal{N}_p(\mathcal{T}_h) \cap \mathbf{H}_0(\mathbf{curl}, \Omega),$$

and we have $\nabla V_h \subset \mathbf{W}_h$. We shall also need the Nédélec and Raviart-Thomas finite element spaces in the metallic part of the domain, namely

$$\mathbf{W}_{m,h} := \mathcal{N}_p(\mathcal{T}_{m,h}) \cap \mathbf{H}_0(\mathbf{curl}, \Omega_m), \quad \mathbf{X}_{m,h} := \mathcal{RT}_p(\mathcal{T}_{m,h}) \cap \mathbf{H}_0(\text{div}, \Omega_m).$$

We have $\nabla \times \mathbf{W}_{m,h} \subset \mathbf{W}_{m,h}$. In addition, if extension by zero is implicitly assume, then $\mathbf{W}_{m,h} \subset \mathbf{W}_h$. We refer the reader to [18] for a detailed description of these finite element spaces.

2.6. Quasi-interpolation operators. Classically, our analysis will rely on “quasi-interpolation” operators [11]. Specifically, there exist four operators $\mathcal{P}_h : H_0^1(\Omega) \rightarrow V_h$, $\mathcal{Q}_h : \mathbf{H}_0(\mathbf{curl}, \Omega) \rightarrow \mathbf{W}_h$, $\mathcal{Q}_{m,h} : \mathbf{H}_0(\mathbf{curl}, \Omega_m) \rightarrow \mathbf{W}_{m,h}$ and $\mathcal{R}_{m,h} : \mathbf{H}_0(\text{div}, \Omega_m) \rightarrow \mathbf{X}_{m,h}$ and a constant \mathcal{C}_{qi} that only depends on the shape-regularity parameter κ such that

$$(2.7a) \quad h_K^{-1} \|q - \mathcal{P}_h q\|_K + h_K^{-1/2} \|q - \mathcal{P}_h q\|_{\partial K} \leq \mathcal{C}_{\text{qi}} \|\nabla q\|_{\tilde{K}},$$

$$(2.7b) \quad h_K^{-1} \|\mathbf{v} - \mathcal{Q}_h \mathbf{v}\|_K + h_K^{-1/2} \|(\mathbf{v} - \mathcal{Q}_h \mathbf{v}) \times \mathbf{n}\|_{\partial K} \leq \mathcal{C}_{\text{qi}} \|\nabla_h \mathbf{v}\|_{\tilde{K}}$$

for all $q \in H_0^1(\Omega)$, $\mathbf{v} \in \mathbf{H}^1(\mathcal{T}_h) \cap \mathbf{H}_0(\mathbf{curl}, \Omega)$ and $K \in \mathcal{T}_h$, as well as

$$(2.7c) \quad h_K^{-1} \|\mathbf{v} - \mathcal{Q}_{m,h} \mathbf{v}\|_K + h_K^{-1/2} \|(\mathbf{v} - \mathcal{Q}_{m,h} \mathbf{v}) \times \mathbf{n}\|_{\partial K} \leq \mathcal{C}_{\text{qi}} \|\nabla_h \mathbf{v}\|_{\tilde{K}_m},$$

$$(2.7d) \quad h_K^{-1} \|\mathbf{w} - \mathcal{R}_{m,h} \mathbf{w}\|_K + h_K^{-1/2} \|(\mathbf{w} - \mathcal{R}_{m,h} \mathbf{w}) \cdot \mathbf{n}\|_{\partial K} \leq \mathcal{C}_{\text{qi}} \|\nabla_h \mathbf{w}\|_{\tilde{K}_m}$$

for all $\mathbf{v} \in \mathbf{H}^1(\mathcal{T}_{m,h}) \cap \mathbf{H}_0(\mathbf{curl}, \Omega_m)$, $\mathbf{w} \in \mathbf{H}^1(\mathcal{T}_{m,h}) \cap \mathbf{H}_0(\text{div}, \Omega_m)$, and $K \in \mathcal{T}_{m,h}$.

2.7. Bubble functions. Classically, we will use “bubble” functions to localize our error analysis. We refer the reader to [26] for a detailed presentation and only state the essential result we need. Given an element $K \in \mathcal{T}_h$ and a face $F \in \mathcal{F}_h$, we denote by $b_K \in H_0^1(K)$ and $b_F \in H_0^1(\tilde{F})$ the element and face bubble functions supported in K and \tilde{F} , respectively. The estimates

$$(2.8a) \quad \|w\|_K \leq \mathcal{C}_b \|b_K^{1/2} w\|_K, \quad \|v\|_F \leq \mathcal{C}_b \|b_F^{1/2} v\|_F$$

hold for all $w \in \mathcal{P}_{p+1}(K)$ and $v \in \mathcal{P}_{p+1}(F)$, where $\mathcal{C}_b > 0$ is a constant depending on the polynomial degree p and the shape regularity parameter κ . Standard inverse inequalities let us conclude that

$$(2.8b) \quad \|\nabla(w b_K)\|_K \leq \mathcal{C}_i h_K^{-1} \|w\|_K \quad \forall w \in \mathcal{P}_{k+1}(K),$$

where again, \mathcal{C}_i only depends on κ and p . We further consider an extension operator $\mathcal{L}_F : \mathcal{P}_{k+1}(F) \rightarrow \mathcal{P}_{p+1}(\tilde{F})$ such that $\mathcal{L}_F(v)|_F = v$ and

$$(2.8c) \quad \|\mathcal{L}_F(v)\|_{\tilde{F}} + h_F \|\nabla(\mathcal{L}_F(v))\|_{\tilde{F}} \leq \mathcal{C}_e h_F^{1/2} \|v\|_F, \quad v \in \mathcal{P}_{k+1}(F),$$

where \mathcal{C}_e depends on β and p . The same results hold true for vector-valued function, as can be seen by applying the scalar estimates componentwise.

2.8. Data oscillation. Our efficiency estimates include a data-oscillation term that we define in this section. We first define a “projected source term” $\pi_h \mathbf{J}_e \in \mathcal{P}_{p+1}(\mathcal{T}_h)$, that is defined for each $K \in \mathcal{T}_h$ as the unique element in $\mathcal{P}_{p+1}(K)$ such that

$$\frac{\omega^2 h_K^2}{c_{E,K}^2} (\pi_h \mathbf{J}_e, \mathbf{v}_h)_K + h_K^2 (\nabla \cdot (\pi_h \mathbf{J}_e), \nabla \cdot \mathbf{v}_h)_K = \frac{\omega^2 h_K^2}{c_{E,K}^2} (\mathbf{J}_e, \mathbf{v}_h)_K + h_K^2 (\nabla \cdot \mathbf{J}_e, \nabla \cdot \mathbf{v}_h)_K$$

for all $\mathbf{v}_h \in \mathcal{P}_{k+1}(K)$. Analogously, we define $\varrho_h \mathbf{K}_e \in \mathcal{P}_{p+1}(\mathcal{T}_h)$, for each $K \in \mathcal{T}_h$, as the unique element in $\mathcal{P}_{p+1}(K)$ such that

$$\frac{\omega^2 h_K^2}{c_{J,K}^2} (\varrho_h \mathbf{K}_e, \mathbf{w}_h)_K + h_K^2 (\nabla \times (\varrho_h \mathbf{K}_e), \nabla \times \mathbf{w}_h)_K = \frac{\omega^2 h_K^2}{c_{J,K}^2} (\mathbf{K}_e, \mathbf{w}_h)_K + h_K^2 (\nabla \times \mathbf{K}_e, \nabla \times \mathbf{w}_h)_K$$

for all $\mathbf{w}_h \in \mathcal{P}_{k+1}(K)$. Then, we may introduce the data oscillation term

$$\begin{aligned} \text{osc}_K^2 &:= \frac{1}{\varepsilon_K^*} \left(\frac{\omega^2 h_K^2}{c_{E,K}^2} \|\mathbf{J}_e - \pi_h \mathbf{J}_e\|_K^2 + h_K^2 \|\nabla \cdot (\mathbf{J}_e - \pi_h \mathbf{J}_e)\|_K^2 \right) \\ &\quad + \frac{1}{\alpha_K^*} \left(\frac{\omega^2 h_K^2}{c_{J,K}^2} \|\mathbf{K}_e - \varrho_h \mathbf{K}_e\|_K^2 + h_K^2 \|\nabla \times (\mathbf{K}_e - \varrho_h \mathbf{K}_e)\|_K^2 \right) \end{aligned}$$

for all $K \in \mathcal{T}_h$, and

$$\text{osc}_{\tilde{K}}^2 := \sum_{K \in \mathcal{T}_h^K} \text{osc}_K^2.$$

Notice that whenever the right-hand side is smooth, namely $\mathbf{J}_e \in \mathbf{H}^{p+1}(\mathcal{T}_h)$, $\nabla \cdot \mathbf{J}_e \in \mathbf{H}^{p+1}(\mathcal{T}_h)$, $\mathbf{K}_e \in \mathbf{H}^{p+1}(\mathcal{T}_h)$ and $\nabla \times \mathbf{K}_e \in \mathbf{H}^{p+1}(\mathcal{T}_h)$, we have $\text{osc}_K = O(h^{p+2})$ for all $K \in \mathcal{T}_h$.

2.9. Regular decomposition. For all $(\mathbf{v}, \mathbf{w}) \in \mathbb{V}$, there exist $q \in H_0^1(\Omega)$, $\boldsymbol{\theta} \in \mathbf{H}^1(\mathcal{T}_{m,h}) \cap \mathbf{H}_0(\text{curl}, \Omega_m)$, $\tilde{\mathbf{v}} \in \mathbf{H}^1(\mathcal{T}_h) \cap \mathbf{H}_0(\text{curl}, \Omega)$ and $\tilde{\mathbf{w}} \in \mathbf{H}^1(\mathcal{T}_{m,h}) \cap \mathbf{H}_0(\text{div}, \Omega_m)$ such that

$$(2.9a) \quad (\mathbf{v}, \mathbf{w}) = (\nabla p + \tilde{\mathbf{v}}, \nabla \times \boldsymbol{\theta} + \tilde{\mathbf{w}})$$

and

$$(2.9b) \quad \omega \|\nabla q\|_{\varepsilon, \Omega} + \omega \|\nabla_h \boldsymbol{\theta}\|_{\alpha, \Omega_m} + \|\nabla_h \tilde{\mathbf{v}}\|_{\chi, \Omega} + \|\nabla_h \tilde{\mathbf{w}}\|_{\zeta, \Omega_m} \leq \mathcal{C}_{\text{rd}} \|(\mathbf{v}, \mathbf{w})\|,$$

where \mathcal{C}_{rd} is a constant that only depends on \mathcal{P} , the ratio between the minimum and maximum value of the coefficients. We refer the reader to Theorems 2 and 6 of [13], as well as [6], Appendix B.

2.10. Inequalities with hidden constants. To simplify the remaining of the exposition, if $A, B \geq 0$ are real numbers, we employ the notation $A \lesssim B$ if there exists a constant C that only depends on $\mathcal{C}_{i/s}$, \mathcal{C}_{qi} , \mathcal{C}_b , \mathcal{C}_e , \mathcal{C}_i , \mathcal{C}_{rd} and the material contrasts such that $A \leq CB$. In particular, C may depend on the geometry of the domain and the material coefficients, the mesh shape-regularity κ and the polynomial degree p , but *not* on the mesh size h .

3. A POSTERIORI ERROR ESTIMATES

3.1. Numerical solution. We are interested in finite element approximations to (2.5). Specifically, we introduce the (conforming) discretization space $\mathbb{V}_h := \mathbf{W}_h \times \mathbf{X}_{m,h}$ and consider an element $(\mathbf{E}_h, \mathbf{J}_h) \in \mathbb{V}_h$ such that

$$(3.1) \quad b((\mathbf{E}_h, \mathbf{J}_h), (\mathbf{v}_h, \mathbf{w}_h)) = i\omega(\mathbf{J}_e, \mathbf{v}_h) + i\omega(\mathbf{K}_e, \mathbf{w}_h) \quad \forall (\mathbf{v}_h, \mathbf{w}_h) \in \mathbb{V}_h.$$

3.2. A posteriori error estimator. We devise a residual-based error estimator. It is based on four terms. The first two are motivated by the two equations of (2.1) and read

$$\begin{aligned} \eta_{\text{curl,curl},K} := & \frac{h_K}{\sqrt{\chi_K^*}} \left\| -\omega^2 \boldsymbol{\varepsilon} \mathbf{E}_h + \nabla \times (\boldsymbol{\chi} \nabla \times \mathbf{E}_h) + i\omega \mathbf{J}_h - i\omega \mathbf{J}_e \right\|_K \\ & + \frac{h_K^{1/2}}{\sqrt{\chi_K^*}} \left\| \llbracket \boldsymbol{\chi} \nabla \times \mathbf{E}_h \rrbracket \times \mathbf{n} \right\|_{\partial K \setminus \partial \Omega} \end{aligned}$$

for all $K \in \mathcal{T}_h$ and

$$\begin{aligned} \eta_{\text{grad,div},K} := & \frac{h_K}{\sqrt{\zeta_K^*}} \left\| -\omega^2 \boldsymbol{\alpha} \mathbf{J}_h - \nabla (\zeta \nabla \cdot \mathbf{J}_h) - i\omega \mathbf{E}_h - i\omega \mathbf{K}_e \right\|_K \\ & + \frac{h_K^{1/2}}{\sqrt{\zeta_K^*}} \left\| \llbracket \zeta \nabla \cdot \mathbf{J}_h \rrbracket \right\|_{\partial K \setminus \partial \Omega_m} \end{aligned}$$

for $K \in \mathcal{T}_{m,h}$. As usual in the context of Maxwell's equations [4, 19], these two terms are insufficient, and we also need to consider the residual terms associated with ‘‘hidden’’ equations (2.2) and (2.3). Hence, we introduce

$$\eta_{\text{div},K} := \frac{h_K}{\sqrt{\varepsilon_K^*}} \left\| \nabla \cdot (i\omega \boldsymbol{\varepsilon} \mathbf{E}_h + \mathbf{J}_h - \mathbf{J}_e) \right\|_K + \frac{\omega h_K^{1/2}}{\sqrt{\varepsilon_K^*}} \left\| \llbracket \boldsymbol{\varepsilon} \mathbf{E}_h \rrbracket \cdot \mathbf{n} \right\|_{\partial K \setminus \partial \Omega}$$

if $K \in \mathcal{T}_h$ and

$$\eta_{\text{curl},K} := \frac{h_K}{\sqrt{\alpha_K^*}} \left\| \nabla \times (i\omega \boldsymbol{\alpha} \mathbf{J}_h - \mathbf{E}_h - \mathbf{K}_e) \right\|_K + \frac{\omega h_K^{1/2}}{\sqrt{\alpha_K^*}} \left\| \llbracket \boldsymbol{\alpha} \mathbf{J}_h \rrbracket \times \mathbf{n} \right\|_{\partial K \setminus \partial \Omega_m}$$

for all $K \in \mathcal{T}_{m,h}$. We then set

$$\eta_K := \eta_{\text{curl,curl},K} + \eta_{\text{grad,div},K} + \eta_{\text{div},K} + \eta_{\text{curl},K},$$

for all $K \in \mathcal{T}_h$ with the implicit convention that $\eta_{\text{grad,div},K} = \eta_{\text{curl},K} = 0$ when $K \notin \mathcal{T}_{m,h}$. Finally,

$$\eta := \left(\sum_{K \in \mathcal{T}_h} \eta_K^2 \right)^{1/2}$$

gathers the elementwise contributions, and we define $\eta_{\text{curl,curl}}$, $\eta_{\text{grad,div}}$, η_{div} and η_{curl} in a similar way.

3.3. Reliability. We first establish that the proposed estimator is reliable. The key ingredient of the proof is to estimate, for an arbitrary element $(\mathbf{v}, \mathbf{w}) \in \mathbb{V}$, the quantity

$$|b((\mathbf{E} - \mathbf{E}_h, \mathbf{J} - \mathbf{J}_h), (\mathbf{v}, \mathbf{w}))|$$

using the estimator η . This is done in four major steps, that are presented in Lemmas 3.1, 3.2, 3.3 and 3.4 below.

Lemma 3.1. *We have*

$$|b((\mathbf{E} - \mathbf{E}_h, \mathbf{J} - \mathbf{J}_h), (\nabla q, \mathbf{o}))| \lesssim \eta_{\text{div}} \omega \|\nabla q\|_{\varepsilon, \Omega}$$

for all $q \in H_0^1(\Omega)$.

Proof. We first observe that

$$\begin{aligned} b((\mathbf{E} - \mathbf{E}_h, \mathbf{J} - \mathbf{J}_h), (\nabla p, \mathbf{o})) &= -\omega^2(\boldsymbol{\varepsilon}(\mathbf{E} - \mathbf{E}_h), \nabla p)_{\mathcal{T}_h} + i\omega(\mathbf{J} - \mathbf{J}_h, \nabla p)_{\mathcal{T}_h} \\ &= i\omega((i\omega\boldsymbol{\varepsilon}\mathbf{E} + \mathbf{J}), \nabla p)_{\mathcal{T}_h} - (i\omega\mathbf{E}_h - \mathbf{J}_h, \nabla p)_{\mathcal{T}_h}. \end{aligned}$$

Then, since $\boldsymbol{\varepsilon}\mathbf{E}, \mathbf{J}, \mathbf{J}_h \in \mathbf{H}_0(\text{div}, \Omega)$ and $p \in H_0^1(\Omega)$, elementwise integration by parts reveals that

$$\begin{aligned} b((\mathbf{E} - \mathbf{E}_h, \mathbf{J} - \mathbf{J}_h), (\nabla p, \mathbf{o})) &= i\omega(-(\nabla \cdot (i\omega\boldsymbol{\varepsilon}\mathbf{E} + \mathbf{J}), p)_{\mathcal{T}_h} + (\nabla \cdot (i\omega\boldsymbol{\varepsilon}\mathbf{E}_h + \mathbf{J}_h), p)_{\mathcal{T}_h}) \\ &\quad - \omega^2\langle \boldsymbol{\varepsilon}\mathbf{E}_h \cdot \mathbf{n}, p \rangle_{\partial\mathcal{T}_h} \\ &= i\omega(\nabla \cdot (i\omega\boldsymbol{\varepsilon}\mathbf{E}_h + \mathbf{J}_h - \mathbf{J}_e), p)_{\mathcal{T}_h} - \omega^2\langle \llbracket \boldsymbol{\varepsilon}\mathbf{E}_h \rrbracket \cdot \mathbf{n}, p \rangle_{\mathcal{F}_h^i}. \end{aligned}$$

Upon rearranging the face sum, it follows that

$$|b((\mathbf{E} - \mathbf{E}_h, \mathbf{J} - \mathbf{J}_h), (\nabla p, \mathbf{o}))| \lesssim \sum_{K \in \mathcal{T}_h} \eta_{\text{div}, K} \omega \sqrt{\varepsilon_K^*} \left(h_K^{-1} \|p\|_K + h_K^{-1/2} \|p\|_{\partial K} \right).$$

Now, let $q \in H_0^1(\Omega)$. Using Galerkin orthogonality (3.1), the inclusion $\nabla V_h \subset \mathbf{W}_h$, and quasi-interpolation estimate (2.7a), we have

$$\begin{aligned} |b((\mathbf{E} - \mathbf{E}_h, \mathbf{J} - \mathbf{J}_h), (\nabla q, \mathbf{o}))| &= |b((\mathbf{E} - \mathbf{E}_h, \mathbf{J} - \mathbf{J}_h), (\nabla(q - \mathcal{P}_h q), \mathbf{o}))| \\ &\lesssim \sum_{K \in \mathcal{T}_h} \eta_{\text{div}, K} \omega \sqrt{\varepsilon_K^*} \left(h_K^{-1} \|q - \mathcal{P}_h q\|_K + h_K^{-1/2} \|q - \mathcal{P}_h q\|_{\partial K} \right) \\ &\lesssim \sum_{K \in \mathcal{T}_h} \eta_{\text{div}, K} \omega \sqrt{\varepsilon_K^*} \|\nabla q\|_{\mathcal{T}_h^K} \lesssim \eta_{\text{div}} \omega \|\nabla q\|_{\varepsilon, \Omega}, \end{aligned}$$

and the result follows. \square

Lemma 3.2. *We have*

$$|b((\mathbf{E} - \mathbf{E}_h, \mathbf{J} - \mathbf{J}_h), (\mathbf{o}, \nabla \times \boldsymbol{\theta}))| \lesssim \eta_{\text{curl}} \omega \|\nabla_h \boldsymbol{\theta}\|_{\alpha, \Omega_m}$$

for all $\boldsymbol{\theta} \in \mathbf{H}^1(\mathcal{T}_{m,h}) \cap \mathbf{H}_0(\text{curl}, \Omega_m)$.

Proof. Let $\boldsymbol{\phi} \in \mathbf{H}^1(\mathcal{T}_{m,h}) \cap \mathbf{H}_0(\text{curl}, \Omega_m)$. The first step of the proof consists in writing that

$$\begin{aligned} b((\mathbf{E} - \mathbf{E}_h, \mathbf{J} - \mathbf{J}_h), (\mathbf{o}, \nabla \times \boldsymbol{\phi})) &= -\omega^2(\boldsymbol{\alpha}(\mathbf{J} - \mathbf{J}_h), \nabla \times \boldsymbol{\phi})_{\Omega_m} - i\omega(\mathbf{E} - \mathbf{E}_h, \nabla \times \boldsymbol{\phi})_{\Omega_m} \\ &= i\omega((i\omega\boldsymbol{\alpha}\mathbf{J} - \mathbf{E}, \nabla \times \boldsymbol{\phi})_{\Omega_m} - (i\omega\boldsymbol{\alpha}\mathbf{J}_h - \mathbf{E}_h, \nabla \times \boldsymbol{\phi})_{\Omega_m}). \end{aligned}$$

Recalling (2.3), integrating by parts over each $K \in \mathcal{T}_{m,h}$ reveals that

$$\begin{aligned} b((\mathbf{E} - \mathbf{E}_h, \mathbf{J} - \mathbf{J}_h), (\mathbf{o}, \nabla \times \boldsymbol{\phi})) &= i\omega((\nabla \times (i\omega\boldsymbol{\alpha}\mathbf{J} - \mathbf{E}), \boldsymbol{\phi})_{\mathcal{T}_{m,h}} - (\nabla \times (i\omega\boldsymbol{\alpha}\mathbf{J}_h - \mathbf{E}_h), \boldsymbol{\phi})_{\mathcal{T}_{m,h}}) \\ &\quad + \omega^2\langle \boldsymbol{\alpha}\mathbf{J}_h \times \mathbf{n}, \boldsymbol{\phi} \rangle_{\partial\mathcal{T}_{m,h}} \\ &= -i\omega(\nabla \times (i\omega\boldsymbol{\alpha}\mathbf{J}_h - \mathbf{E}_h - \mathbf{K}_e), \boldsymbol{\phi})_{\mathcal{T}_{m,h}} + \omega^2\langle \boldsymbol{\alpha}\mathbf{J}_h \times \mathbf{n}, \boldsymbol{\phi} \rangle_{\partial\mathcal{T}_{m,h}} \\ &= -i\omega(\nabla_h \times (i\omega\boldsymbol{\alpha}\mathbf{J}_h - \mathbf{E}_h - \mathbf{K}_e), \boldsymbol{\phi})_{\Omega_m} + \omega^2\langle \llbracket \boldsymbol{\alpha}\mathbf{J}_h \rrbracket \times \mathbf{n}, \boldsymbol{\phi} \rangle_{\mathcal{F}_{m,h}}, \end{aligned}$$

and

$$|b((\mathbf{E} - \mathbf{E}_h, \mathbf{J} - \mathbf{J}_h), (\mathbf{o}, \nabla \times \boldsymbol{\phi}))| \lesssim \sum_{K \in \mathcal{T}_{m,h}} \eta_{\text{curl}, K} \omega \sqrt{\alpha_K^*} \left(h_K^{-1} \|\boldsymbol{\phi}\|_K + h_K^{-1/2} \|\boldsymbol{\phi}\|_{\partial K} \right).$$

Let $\boldsymbol{\theta} \in \mathbf{H}^1(\mathcal{T}_{m,h}) \cap \mathbf{H}_0(\mathbf{curl}, \Omega_m)$. Then, recalling Galerkin orthogonality (3.1), that $\nabla \times \mathbf{W}_{m,h} \subset \mathbf{X}_{m,h}$ and (2.7c), we have

$$\begin{aligned} |b((\mathbf{E} - \mathbf{E}_h, \mathbf{J} - \mathbf{J}_h), (\boldsymbol{o}, \nabla \times \boldsymbol{\theta}))| &= |b((\mathbf{E} - \mathbf{E}_h, \mathbf{J} - \mathbf{J}_h), (\boldsymbol{o}, \nabla \times (\boldsymbol{\theta} - \mathcal{Q}_{m,h}\boldsymbol{\theta}))| \\ &\lesssim \sum_{K \in \mathcal{T}_{m,h}} \eta_{\mathbf{curl},K} \omega \sqrt{\alpha_K^*} \left(h_K^{-1} \|\boldsymbol{\theta} - \mathcal{Q}_{m,h}\boldsymbol{\theta}\|_K + h_K^{-1/2} \|(\boldsymbol{\theta} - \mathcal{Q}_{m,h}\boldsymbol{\theta}) \times \mathbf{n}\|_{\partial K} \right) \\ &\lesssim \sum_{K \in \mathcal{T}_{m,h}} \eta_{\mathbf{curl},K} \omega \sqrt{\alpha_K^*} \|\nabla \boldsymbol{\theta}\|_{\mathcal{T}_{m,h}^K} \lesssim \eta_{\mathbf{curl}} \omega \|\nabla \boldsymbol{\theta}\|_{\alpha, \mathcal{T}_{m,h}}. \end{aligned}$$

□

Lemma 3.3. *We have*

$$|b((\mathbf{E} - \mathbf{E}_h, \mathbf{J} - \mathbf{J}_h), (\tilde{\mathbf{v}}, \boldsymbol{o}))| \lesssim \eta_{\mathbf{curl},\mathbf{curl}} \|\nabla_h \tilde{\mathbf{v}}\|_{\chi, \Omega}$$

for all $\tilde{\mathbf{v}} \in \mathbf{H}^1(\mathcal{T}_h) \cap \mathbf{H}_0(\mathbf{curl}, \Omega)$.

Proof. Let $\boldsymbol{\phi} \in \mathbf{H}^1(\mathcal{T}_h) \cap \mathbf{H}_0(\mathbf{curl}, \Omega)$. We have

$$b((\mathbf{E} - \mathbf{E}_h, \mathbf{J} - \mathbf{J}_h), (\boldsymbol{\phi}, \boldsymbol{o})) = i\omega(\mathbf{J}_e, \boldsymbol{\phi}) - b((\mathbf{E}_h, \mathbf{J}_h), (\boldsymbol{\phi}, \boldsymbol{o})),$$

and

$$\begin{aligned} b((\mathbf{E}_h, \mathbf{J}_h), (\boldsymbol{\phi}, \boldsymbol{o})) &= -\omega^2(\boldsymbol{\varepsilon}\mathbf{E}_h, \boldsymbol{\phi})_{\mathcal{T}_h} + (\boldsymbol{\chi}\nabla \times \mathbf{E}_h, \nabla \times \boldsymbol{\phi})_{\mathcal{T}_h} + i\omega(\mathbf{J}, \boldsymbol{\phi})_{\mathcal{T}_h} \\ &= (-\omega^2\boldsymbol{\varepsilon}\mathbf{E}_h + \nabla \times (\boldsymbol{\chi}\nabla \times \mathbf{E}_h) + i\omega\mathbf{J}_h, \boldsymbol{\phi})_{\mathcal{T}_h} + \langle (\boldsymbol{\chi}\nabla \times \mathbf{E}_h) \times \mathbf{n}, \boldsymbol{\phi} \rangle_{\partial\mathcal{T}_h}. \end{aligned}$$

It follows that

$$\begin{aligned} b((\mathbf{E} - \mathbf{E}_h, \mathbf{J} - \mathbf{J}_h), (\boldsymbol{\phi}, \boldsymbol{o})) &= -(-\omega^2\boldsymbol{\varepsilon}\mathbf{E}_h + \nabla_h \times (\boldsymbol{\chi}\nabla \times \mathbf{E}_h) + i\omega\mathbf{J}_h - i\omega\mathbf{J}_e, \boldsymbol{\phi})_{\Omega} + \langle [\boldsymbol{\chi}\nabla \times \mathbf{E}_h] \times \mathbf{n}, \boldsymbol{\phi} \rangle_{\mathcal{F}_h}, \end{aligned}$$

and

$$|b((\mathbf{E} - \mathbf{E}_h, \mathbf{J} - \mathbf{J}_h), (\boldsymbol{\phi}, \boldsymbol{o}))| \lesssim \sum_{K \in \mathcal{T}_h} \eta_{\mathbf{curl},\mathbf{curl},K} \sqrt{\chi_K^*} \left(h_K^{-1} \|\boldsymbol{\phi}\|_K + h_K^{-1/2} \|\boldsymbol{\phi} \times \mathbf{n}\|_{\partial K} \right).$$

Then, we consider $\tilde{\mathbf{v}} \in \mathbf{H}^1(\mathcal{T}_h) \cap \mathbf{H}_0(\mathbf{curl}, \Omega)$ and conclude the proof thanks to Galerkin orthogonality (3.1) and estimate (2.7b), since

$$\begin{aligned} |b((\mathbf{E} - \mathbf{E}_h, \mathbf{J} - \mathbf{J}_h), (\tilde{\mathbf{v}}, \boldsymbol{o}))| &= |b((\mathbf{E} - \mathbf{E}_h, \mathbf{J} - \mathbf{J}_h), (\tilde{\mathbf{v}} - \mathcal{Q}_h\tilde{\mathbf{v}}, \boldsymbol{o}))| \\ &\lesssim \sum_{K \in \mathcal{T}_h} \eta_{\mathbf{curl},\mathbf{curl},K} \sqrt{\chi_K^*} \left(h_K^{-1} \|\tilde{\mathbf{v}} - \mathcal{Q}_h\tilde{\mathbf{v}}\|_K + h_K^{-1/2} \|(\tilde{\mathbf{v}} - \mathcal{Q}_h\tilde{\mathbf{v}}) \times \mathbf{n}\|_{\partial K} \right) \\ &\lesssim \sum_{K \in \mathcal{T}_h} \eta_{\mathbf{curl},\mathbf{curl},K} \sqrt{\chi_K^*} \|\nabla_h \tilde{\mathbf{v}}\|_{\tilde{K}} \lesssim \eta_{\mathbf{curl},\mathbf{curl}} \|\nabla_h \tilde{\mathbf{v}}\|_{\chi, \Omega}. \end{aligned}$$

□

Lemma 3.4. *We have*

$$|b((\mathbf{E} - \mathbf{E}_h, \mathbf{J} - \mathbf{J}_h), (\boldsymbol{o}, \tilde{\mathbf{w}}))| \lesssim \eta_{\mathbf{grad},\mathbf{div}} \|\nabla \tilde{\mathbf{w}}\|_{\zeta, \mathcal{T}_{m,h}}$$

for all $\tilde{\mathbf{w}} \in \mathbf{H}^1(\mathcal{T}_{m,h}) \cap \mathbf{H}_0(\mathbf{div}, \Omega_m)$.

Proof. Let $\phi \in \mathbf{H}^1(\mathcal{T}_{m,h}) \cap \mathbf{H}_0(\text{div}, \Omega_m)$. Then, we have

$$\begin{aligned} b((\mathbf{E} - \mathbf{E}_h, \mathbf{J} - \mathbf{J}_h), (\mathbf{o}, \phi)) &= i\omega(\mathbf{K}_e, \phi)_{\mathcal{T}_{m,h}} + \omega^2(\boldsymbol{\alpha}\mathbf{J}_h, \phi)_{\mathcal{T}_{m,h}} - (\zeta \nabla \cdot \mathbf{J}_h, \nabla \cdot \phi)_{\mathcal{T}_{m,h}} + i\omega(\mathbf{E}_h, \phi)_{\mathcal{T}_{m,h}} \\ &= -(-\omega^2 \boldsymbol{\alpha}\mathbf{J}_h - \nabla(\zeta \nabla \cdot \mathbf{J}_h) - i\omega \mathbf{E}_h - i\omega \mathbf{K}_e, \phi)_{\mathcal{T}_{m,h}} - \langle \zeta \nabla \cdot \mathbf{J}_h, \phi \cdot \mathbf{n} \rangle_{\partial \mathcal{T}_{m,h}} \\ &= -(-\omega^2 \boldsymbol{\alpha}\mathbf{J}_h - \nabla(\zeta \nabla \cdot \mathbf{J}_h) - i\omega \mathbf{E}_h - i\omega \mathbf{K}_e, \phi)_{\mathcal{T}_{m,h}} - (\llbracket \zeta \nabla \cdot \mathbf{J}_h \rrbracket, \phi \cdot \mathbf{n})_{\mathcal{F}_{m,h}^i} \end{aligned}$$

and

$$|b((\mathbf{E} - \mathbf{E}_h, \mathbf{J} - \mathbf{J}_h), (\mathbf{o}, \phi))| \lesssim \sum_{K \in \mathcal{T}_{m,h}} \eta_{\text{grad,div},K} \sqrt{\zeta_K^*} \left(h_K^{-1} \|\phi\|_K + h_K^{-1/2} \|\phi\|_{\partial K} \right).$$

Now, let $\tilde{\mathbf{w}} \in \mathbf{H}^1(\mathcal{T}_{m,h}) \cap \mathbf{H}_0(\text{div}, \Omega_m)$. By Galerkin orthogonality and the estimate (2.7d), we conclude

$$\begin{aligned} |b((\mathbf{E} - \mathbf{E}_h, \mathbf{J} - \mathbf{J}_h), (\mathbf{o}, \tilde{\mathbf{w}}))| &= |b((\mathbf{E} - \mathbf{E}_h, \mathbf{J} - \mathbf{J}_h), (\mathbf{o}, \tilde{\mathbf{w}} - \mathcal{R}_{m,h}\tilde{\mathbf{w}}))| \\ &\lesssim \sum_{K \in \mathcal{T}_{m,h}} \eta_{\text{grad,div},K} \sqrt{\zeta_K^*} \left(h_K^{-1} \|\tilde{\mathbf{w}} - \mathcal{R}_{m,h}\tilde{\mathbf{w}}\|_K + h_K^{-1/2} \|(\tilde{\mathbf{w}} - \mathcal{R}_{m,h}\tilde{\mathbf{w}}) \cdot \mathbf{n}\|_{\partial K} \right) \\ &\lesssim \sum_{K \in \mathcal{T}_{m,h}} \eta_{\text{grad,div},K} \sqrt{\zeta_K^*} \|\nabla \tilde{\mathbf{w}}\|_{\mathcal{T}_{m,h}^K} \lesssim \eta_{\text{grad,div}} \|\nabla \tilde{\mathbf{w}}\|_{\zeta, \mathcal{T}_{m,h}}. \end{aligned}$$

□

We now establish that the proposed estimator is reliable in Theorem 3.5. The proof builds upon Lemmas 3.1, 3.2, 3.3 and 3.4 combined with inf-sup condition (2.6) and regular decomposition (2.9).

Theorem 3.5. *We have*

$$(3.2) \quad \|\mathbf{E} - \mathbf{E}_h, \mathbf{J} - \mathbf{J}_h\| \lesssim \eta.$$

Proof. Since \mathbb{V} in a Hilbert space, it follows from inf-sup condition (2.6) that there exists $(\mathbf{v}^*, \mathbf{w}^*) \in \mathbb{V}$ with $\|(\mathbf{v}^*, \mathbf{w}^*)\| = 1$ such that

$$\|\mathbf{E} - \mathbf{E}_h, \mathbf{J} - \mathbf{J}_h\| \leq \mathcal{C}_{i/s}^{-1} \text{Re } b((\mathbf{E} - \mathbf{E}_h, \mathbf{J} - \mathbf{J}_h), \mathbf{v}^*, \mathbf{w}^*).$$

Then, using (2.9), we have

$$\mathbf{v}^* = \tilde{\mathbf{v}} + \nabla p, \quad \mathbf{w}^* = \tilde{\mathbf{w}} + \nabla \times \boldsymbol{\theta},$$

where $\tilde{\mathbf{v}} \in \mathbf{H}^1(\mathcal{T}_h) \cap \mathbf{H}_0(\text{curl}, \Omega)$, $p \in H_0^1(\Omega)$, $\tilde{\mathbf{w}} \in \mathbf{H}^1(\mathcal{T}_{m,h}) \cap \mathbf{H}_0(\text{div}, \Omega_m)$ and $\boldsymbol{\theta} \in \mathbf{H}^1(\mathcal{T}_{m,h}) \cap \mathbf{H}_0(\text{curl}, \Omega_m)$ with

$$\omega \|\nabla q\|_{\varepsilon, \Omega} + \omega \|\nabla_h \boldsymbol{\theta}\|_{\alpha, \Omega_m} + \|\nabla_h \tilde{\mathbf{v}}\|_{\chi, \Omega} + \|\nabla_h \tilde{\mathbf{w}}\|_{\zeta, \Omega_m} \lesssim \|(\mathbf{v}^*, \mathbf{w}^*)\| = 1,$$

and (3.2) follows by linearity and the estimates established in Lemma 3.1, 3.2, 3.3 and 3.4. □

3.4. Efficiency. We show that the proposed estimator is efficient. To this end, we establish four results that provide upper bounds for each of the four terms constituting our estimator.

Lemma 3.6. *The estimate*

$$(3.3) \quad \eta_{\text{div},K} \lesssim (1 + k_{P,K} h_K) \|\mathbf{E} - \mathbf{E}_h, \mathbf{J} - \mathbf{J}_h\|_{\tilde{K}} + \text{osc}_{\tilde{K}},$$

holds true for all $K \in \mathcal{T}_h$.

Proof. Using (2.4), we first record that the estimate

$$(3.4) \quad \frac{h_K}{\sqrt{\varepsilon_K^*}} \|\nabla \cdot (\mathbf{J} - \mathbf{J}_h)\|_K \lesssim k_{P,K} h_K \|(\mathbf{E} - \mathbf{E}_h, \mathbf{J} - \mathbf{J}_h)\|_K,$$

holds true for any $K \in \mathcal{T}_h$.

We then fix $K \in \mathcal{T}_h$, and introduce the notations $\mathbf{r}_K := i\omega\varepsilon\mathbf{E}_h + \mathbf{J}_h - \mathbf{J}_e$ and $\mathbf{r}_K^h := \pi_h \mathbf{r}_K$. Recalling (2.2), we have

$$-\nabla \cdot \mathbf{r}_K^h = i\omega \nabla \cdot (\varepsilon(\mathbf{E} - \mathbf{E}_h)) + \nabla \cdot (\mathbf{J} - \mathbf{J}_h) - \nabla \cdot (\mathbf{J}_e - \pi_h \mathbf{J}_e),$$

and thanks to (2.8a)

$$(3.5) \quad \begin{aligned} \|\nabla \cdot \mathbf{r}_K^h\|_{0,K}^2 &\lesssim |(b_K \nabla \cdot \mathbf{r}_K^h, \nabla \cdot \mathbf{r}_K^h)_K| \\ &\lesssim |(b_K \nabla \cdot \mathbf{r}_K^h, \nabla \cdot (i\omega\varepsilon(\mathbf{E} - \mathbf{E}_h)))_K| + |(b_K \nabla \cdot \mathbf{r}_K^h, \nabla \cdot (\mathbf{J} - \mathbf{J}_h) + \nabla \cdot (\mathbf{J}_e - \pi_h \mathbf{J}_e))_K|. \end{aligned}$$

Then, we use (2.8b) to estimate the two terms in the right-hand side of (3.5) with

$$|(b_K \nabla \cdot \mathbf{r}_K^h, \nabla \cdot (i\omega\varepsilon(\mathbf{E} - \mathbf{E}_h)))_K| = |(\nabla(b_K \nabla \cdot \mathbf{r}_K^h), \omega\varepsilon(\mathbf{E} - \mathbf{E}_h))_K| \lesssim h_K^{-1} \|\nabla \cdot \mathbf{r}_K^h\| \|\omega\varepsilon(\mathbf{E} - \mathbf{E}_h)\|_K$$

and

$$|(b_K \nabla \cdot \mathbf{r}_K^h, \nabla \cdot (\mathbf{J} - \mathbf{J}_h) + \nabla \cdot (\mathbf{J}_e - \pi_h \mathbf{J}_e))_K| \lesssim \|\nabla \cdot \mathbf{r}_K^h\|_K (\|\nabla \cdot (\mathbf{J} - \mathbf{J}_h)\|_K + \|\nabla \cdot (\mathbf{J}_e - \pi_h \mathbf{J}_e)\|_K),$$

and it follows that

$$\frac{h_K}{\sqrt{\varepsilon_K^*}} \|\nabla \cdot \mathbf{r}_K^h\|_K \lesssim \omega \|\mathbf{E} - \mathbf{E}_h\|_{\varepsilon,K} + \frac{h_K}{\sqrt{\varepsilon_K^*}} \|\nabla \cdot (\mathbf{J} - \mathbf{J}_h)\|_K + \frac{h_K}{\sqrt{\varepsilon_K^*}} \|\nabla \cdot (\mathbf{J}_e - \pi_h \mathbf{J}_e)\|_K.$$

After observing $\mathbf{r}_K^h - \mathbf{r}_K = \mathbf{J}_e - \pi_h \mathbf{J}_e$, we conclude that

$$(3.6) \quad \frac{h_K}{\sqrt{\varepsilon_K^*}} \|\nabla \cdot \mathbf{r}_K\|_K \lesssim (1 + k_{P,K} h_K) \|(\mathbf{E} - \mathbf{E}_h, \mathbf{J} - \mathbf{J}_h)\|_K + \text{osc}_K.$$

Now, if $F \in \mathcal{F}_K$, we let $w_F := b_F \mathcal{L}_F(\llbracket \varepsilon \mathbf{E}_h \rrbracket \cdot \mathbf{n}_F)$. Since $\varepsilon \mathbf{E} \in \mathbf{H}(\text{div}, \tilde{F})$ and $w_F \in H_0^1(\tilde{F})$, we can employ integration by parts and (2.8a) to show that

$$\|\llbracket \varepsilon \mathbf{E}_h \rrbracket \cdot \mathbf{n}_F\|_F^2 \lesssim |\langle \llbracket \varepsilon \mathbf{E}_h \rrbracket \cdot \mathbf{n}_F, w_F \rangle_F| = |(\varepsilon(\mathbf{E} - \mathbf{E}_h), \nabla w_F)_{\tilde{F}} + (\nabla_h \cdot (\varepsilon(\mathbf{E} - \mathbf{E}_h)), w_F)_{\tilde{F}}|,$$

and it follows from (2.8c) that

$$(3.7) \quad \frac{\omega h_K^{1/2}}{\sqrt{\varepsilon_K^*}} \|\llbracket \varepsilon \mathbf{E}_h \rrbracket \cdot \mathbf{n}_F\|_F \lesssim \omega \|\mathbf{E} - \mathbf{E}_h\|_{\varepsilon, \tilde{F}} + \frac{\omega h_K}{\sqrt{\varepsilon_K^*}} \|\nabla_h \cdot (\varepsilon(\mathbf{E} - \mathbf{E}_h))\|_{\tilde{F}}.$$

Recalling (2.2), we have

$$\nabla_h \cdot (i\omega\varepsilon(\mathbf{E} - \mathbf{E}_h)) = \nabla_h \cdot (i\omega\varepsilon\mathbf{E}_h + \mathbf{J}_h - \mathbf{J}_e) + \nabla \cdot (\mathbf{J} - \mathbf{J}_h),$$

and (2.4), (3.4) as well as (3.6) show that

$$(3.8) \quad \frac{\omega h_K}{\sqrt{\varepsilon_K^*}} \|\nabla_h \cdot (\varepsilon(\mathbf{E} - \mathbf{E}_h))\|_{\tilde{F}} \lesssim (1 + k_{P,K} h_K) \|(\mathbf{E} - \mathbf{E}_h, \mathbf{J} - \mathbf{J}_h)\|_{\tilde{F}} + \text{osc}_{\tilde{K}}.$$

Then, (3.3) follows from (3.6), (3.7) and (3.8). \square

Lemma 3.7. *The estimate*

$$(3.9) \quad \eta_{\text{curl},K} \lesssim \left(1 + \frac{c_{J,K}}{c_{E,K}} k_{P,K} h_K\right) \|(\mathbf{E} - \mathbf{E}_h, \mathbf{J} - \mathbf{J}_h)\|_{\tilde{K}}$$

holds true for all $K \in \mathcal{T}_h$.

Proof. Thanks to (2.3), (2.8a) and after integrating by parts, we obtain that

$$(3.10) \quad \begin{aligned} & \|\nabla \times (i\omega\alpha\mathbf{J}_h - \mathbf{E}_h - \varrho_h\mathbf{K}_e)\|_K^2 \\ & \lesssim |(b_K\nabla \times (i\omega\alpha\mathbf{J}_h - \mathbf{E}_h - \varrho_h\mathbf{K}_e), \nabla \times (i\omega\alpha\mathbf{J}_h - \mathbf{E}_h - \varrho_h\mathbf{K}_e))_K| \\ & \leq |(\nabla \times (b_K\nabla \times (i\omega\alpha\mathbf{J}_h - \mathbf{E}_h - \varrho_h\mathbf{K}_e)), i\omega\alpha(\mathbf{J} - \mathbf{J}_h))_K| \\ & \quad + |(b_K\nabla \times (i\omega\alpha\mathbf{J}_h - \mathbf{E}_h - \varrho_h\mathbf{K}_e), \nabla \times (\mathbf{E} - \mathbf{E}_h) + \nabla \times (\mathbf{K}_e - \varrho_h\mathbf{K}_e))_K| \end{aligned}$$

for all $K \in \mathcal{T}_h$.

Now, for the terms in the right-hand side of (3.10), we use (2.8b) and have

$$|(\nabla \times (b_K\nabla \times (i\omega\alpha\mathbf{J}_h - \mathbf{E}_h - \varrho_h\mathbf{K}_e)), i\omega\alpha(\mathbf{J} - \mathbf{J}_h))_K| \lesssim h_K^{-1} \|\nabla \times (i\omega\alpha\mathbf{J}_h - \mathbf{E}_h - \varrho_h\mathbf{K}_e)\|_K \omega \|\alpha(\mathbf{J} - \mathbf{J}_h)\|_K$$

and

$$\begin{aligned} & |(b_K\nabla \times (i\omega\alpha\mathbf{J}_h - \mathbf{E}_h - \varrho_h\mathbf{K}_e), \nabla \times (\mathbf{E} - \mathbf{E}_h) + \nabla \times (\mathbf{K}_e - \varrho_h\mathbf{K}_e))_K| \\ & \lesssim \|\nabla \times (i\omega\alpha\mathbf{J}_h - \mathbf{E}_h - \varrho_h\mathbf{K}_e)\|_K \|\nabla \times (\mathbf{E} - \mathbf{E}_h)\|_K \\ & \quad + \|\nabla \times (i\omega\alpha\mathbf{J}_h - \mathbf{E}_h - \varrho_h\mathbf{K}_e)\|_K \|\nabla \times (\mathbf{K}_e - \varrho_h\mathbf{K}_e)\|_K. \end{aligned}$$

Then,

$$\begin{aligned} & \frac{h_K}{\sqrt{\alpha_K^*}} \|\nabla \times (i\omega\alpha\mathbf{J}_h - \mathbf{E}_h - \varrho_h\mathbf{K}_e)\|_K \lesssim \\ & \quad \omega \|\mathbf{J} - \mathbf{J}_h\|_{\alpha,K} + \frac{h_K}{\sqrt{\chi_K^* \alpha_K^*}} \|\nabla \times (\mathbf{E} - \mathbf{E}_h)\|_{\chi,K} + \frac{h_K}{\sqrt{\chi_K^* \alpha_K^*}} \|\nabla \times (\mathbf{K}_e - \varrho_h\mathbf{K}_e)\|_{\chi,K}, \end{aligned}$$

and recalling (2.4), we conclude that

$$(3.11) \quad \frac{h_K}{\sqrt{\alpha_K^*}} \|\nabla \times (i\omega\alpha\mathbf{J}_h - \mathbf{E}_h - \mathbf{K}_e)\|_K \lesssim \left(1 + \frac{c_{J,K}}{c_{E,K}} k_{P,K} h_K\right) \|(\mathbf{E} - \mathbf{E}_h, \mathbf{J} - \mathbf{J}_h)\|_K + \text{osc}_K.$$

On the other hand, for a fixed $K \in \mathcal{T}_h$, if $F \in \mathcal{F}_K$ we set $\mathbf{w}_F := b_F \mathcal{L}_F(\llbracket \alpha\mathbf{J}_h \rrbracket \times \mathbf{n}_F)$. Recalling that $\alpha\mathbf{J} \in \mathbf{H}(\text{curl}, \tilde{F})$ and $b_F \in H_0^1(\tilde{F})$, and using (2.8a), we have

$$\begin{aligned} \|\llbracket \alpha\mathbf{J}_h \rrbracket \times \mathbf{n}_F\|_F^2 & \lesssim |\langle \llbracket \alpha\mathbf{J}_h \rrbracket \times \mathbf{n}_F, \mathbf{w}_F \rangle_F| \\ & = |(\alpha(\mathbf{J} - \mathbf{J}_h), \nabla \times \mathbf{w}_F)_{\tilde{F}} + (\nabla \times (\alpha(\mathbf{J} - \mathbf{J}_h)), \mathbf{w}_F)_{\tilde{F}}|, \end{aligned}$$

and thanks to (2.8c), we get that

$$(3.12) \quad \frac{\omega h_K^{1/2}}{\sqrt{\alpha_K^*}} \|\llbracket \alpha\mathbf{J}_h \rrbracket \times \mathbf{n}_F\|_F \lesssim \omega \|\mathbf{J} - \mathbf{J}_h\|_{\alpha, \tilde{F}} + \frac{\omega h_K}{\sqrt{\alpha_K^*}} \|\nabla \times (\alpha(\mathbf{J} - \mathbf{J}_h))\|_{\tilde{F}}.$$

Invoking (2.3), we have

$$\nabla \times (i\omega\alpha(\mathbf{J} - \mathbf{J}_h)) = -\nabla \times (i\omega\alpha\mathbf{J}_h - \mathbf{E}_h - \mathbf{K}_e) + \nabla \times (\mathbf{E} - \mathbf{E}_h)$$

and then, (2.4) and (3.11) let us conclude that

$$(3.13) \quad \frac{\omega h_K}{\sqrt{\alpha_K^*}} \|\nabla \times (\boldsymbol{\alpha}(\mathbf{J} - \mathbf{J}_h))\|_{\tilde{F}} \lesssim \left(1 + \frac{c_{J,K}}{c_{E,K}} k_{P,K} h_K\right) \|(\mathbf{E} - \mathbf{E}_h, \mathbf{J} - \mathbf{J}_h)\|_{\tilde{F}} + \text{osc}_{\tilde{K}}.$$

Finally, (3.9) follows from (3.11), (3.12) and (3.13). \square

Lemma 3.8. *The estimate*

$$(3.14) \quad \eta_{\text{curl,curl},K} \lesssim \left(1 + \left(k_{E,K} + \frac{c_{J,K}}{c_{E,K}} k_{P,K}\right) h_K\right) \|(\mathbf{E} - \mathbf{E}_h, \mathbf{J} - \mathbf{J}_h)\|_{\tilde{K}} + \text{osc}_{\tilde{K}}$$

holds true for all $K \in \mathcal{T}_h$.

Proof. For a fixed $K \in \mathcal{T}_h$, we set $\mathbf{r}_K := -\omega^2 \boldsymbol{\varepsilon} \mathbf{E}_h + \nabla \times (\boldsymbol{\chi} \nabla \times \mathbf{E}_h) + i\omega \mathbf{J}_h - i\omega \mathbf{J}_e$ and $\mathbf{r}_K^h := \pi_h \mathbf{r}_K$. Then, considering (2.1), (2.8a) and integrating by parts, we get

$$(3.15) \quad \begin{aligned} \|\mathbf{r}_K^h\|_K^2 &\lesssim |(\mathbf{r}_K^h, b_K \mathbf{r}_K^h)_K| \\ &\lesssim |(\omega^2 \boldsymbol{\varepsilon}(\mathbf{E} - \mathbf{E}_h), b_K \mathbf{r}_K^h)_K| + |(\boldsymbol{\chi} \nabla \times (\mathbf{E} - \mathbf{E}_h), \nabla \times (b_K \mathbf{r}_K^h))_K| \\ &\quad + |(i\omega(\mathbf{J} - \mathbf{J}_h), b_K \mathbf{r}_K^h)_K| + |(i\omega(\mathbf{J}_e - \pi_h \mathbf{J}_e), b_K \mathbf{r}_K^h)_K|. \end{aligned}$$

To bound the right-hand side terms in (3.15), we use (2.8b) to obtain

$$\begin{aligned} |(\omega^2 \boldsymbol{\varepsilon}(\mathbf{E} - \mathbf{E}_h), b_K \mathbf{r}_K^h)_K| &\lesssim \omega^2 \|\boldsymbol{\varepsilon}(\mathbf{E} - \mathbf{E}_h)\|_K \|\mathbf{r}_K^h\|_K, \\ |(\boldsymbol{\chi} \nabla \times (\mathbf{E} - \mathbf{E}_h), \nabla \times (b_K \mathbf{r}_K^h))_K| &\lesssim h_K^{-1} \|\boldsymbol{\chi} \nabla \times (\mathbf{E} - \mathbf{E}_h)\|_K \|\mathbf{r}_K^h\|_K, \\ |(i\omega(\mathbf{J} - \mathbf{J}_h), b_K \mathbf{r}_K^h)_K| &\lesssim \omega \|\mathbf{J} - \mathbf{J}_h\|_K \|\mathbf{r}_K^h\|_K, \\ |(i\omega(\mathbf{J}_e - \pi_h \mathbf{J}_e), b_K \mathbf{r}_K^h)_K| &\lesssim \omega \|\mathbf{J}_e - \pi_h \mathbf{J}_e\|_K \|\mathbf{r}_K^h\|_K, \end{aligned}$$

and we have that

$$\frac{h_K}{\sqrt{\chi_K^*}} \|\mathbf{r}_K^h\|_K \lesssim \frac{\omega^2 h_K}{\sqrt{\chi_K^*}} \|\boldsymbol{\varepsilon}(\mathbf{E} - \mathbf{E}_h)\|_K + \frac{1}{\sqrt{\chi_K^*}} \|\boldsymbol{\chi} \nabla \times (\mathbf{E} - \mathbf{E}_h)\|_K + \frac{\omega h_K}{\sqrt{\chi_K^*}} \|\mathbf{J} - \mathbf{J}_h\|_K + \text{osc}_K.$$

Noticing that $\mathbf{r}_K^h - \mathbf{r}_K = i\omega(\mathbf{J}_e - \pi_h \mathbf{J}_e)$ and recalling (2.4), we get

$$(3.16) \quad \frac{h_K}{\sqrt{\chi_K^*}} \|\mathbf{r}_K\|_K \lesssim \left(1 + \left(k_{E,K} + \frac{c_{J,K}}{c_{E,K}} k_{P,K}\right) h_K\right) \|(\mathbf{E} - \mathbf{E}_h, \mathbf{J} - \mathbf{J}_h)\|_K + \text{osc}_K.$$

Now, for $F \in \mathcal{F}_h$, we define $\mathbf{w}_F := b_F \mathcal{L}_F([\boldsymbol{\varepsilon} \mathbf{E}_h] \cdot \mathbf{n}_F)$. Since $\boldsymbol{\chi} \nabla \times \mathbf{E} \in \mathbf{H}(\text{curl}, \tilde{F})$ and $\mathbf{w}_F \in \mathbf{H}_0^1(\tilde{F})$, using (2.8a) and integrating by parts, we see that

$$\begin{aligned} \|[\boldsymbol{\chi} \nabla \times \mathbf{E}_h] \times \mathbf{n}_F\|_F^2 &\lesssim |\langle [\boldsymbol{\chi} \nabla \times \mathbf{E}_h] \times \mathbf{n}_F, \mathbf{w}_F \rangle_F| \\ &= |(\nabla \times (\boldsymbol{\chi} \nabla \times (\mathbf{E} - \mathbf{E}_h)), \mathbf{w}_F)_{\tilde{F}} - (\boldsymbol{\chi} \nabla \times (\mathbf{E} - \mathbf{E}_h), \nabla \times \mathbf{w}_F)_{\tilde{F}}|. \end{aligned}$$

Thanks to (2.1), we deduce that

$$\begin{aligned} \|[\boldsymbol{\chi} \nabla \times \mathbf{E}_h] \times \mathbf{n}_F\|_F^2 &\lesssim |(\omega^2 \boldsymbol{\varepsilon}(\mathbf{E} - \mathbf{E}_h), \mathbf{w}_F)_{\tilde{F}} - (\boldsymbol{\chi} \nabla \times (\mathbf{E} - \mathbf{E}_h), \nabla \times \mathbf{w}_F)_{\tilde{F}} \\ &\quad - (i\omega(\mathbf{J} - \mathbf{J}_h), \mathbf{w}_F)_{\tilde{F}} + (\mathbf{r}_K, \mathbf{w}_K)_{\tilde{F}}| \end{aligned}$$

and then, thanks to (2.8c), we have that

$$\begin{aligned} \frac{h_K^{1/2}}{\sqrt{\chi_K^*}} \|\llbracket \boldsymbol{\chi} \nabla \times \mathbf{E}_h \rrbracket \times \mathbf{n}_F\|_F &\lesssim \frac{\omega^2 h_K}{\sqrt{\chi_K^*}} \|\boldsymbol{\varepsilon}(\mathbf{E} - \mathbf{E}_h)\|_{\tilde{F}} + \frac{1}{\sqrt{\chi_K^*}} \|\boldsymbol{\chi} \nabla \times (\mathbf{E} - \mathbf{E}_h)\|_{\tilde{F}} \\ &+ \frac{\omega h_K}{\sqrt{\chi_K^*}} \|\mathbf{J} - \mathbf{J}_h\|_{\tilde{F}} + \frac{h_K}{\sqrt{\chi_K^*}} \|\mathbf{r}_K\|_{\tilde{F}}. \end{aligned}$$

Finally, (2.4) shows that

$$(3.17) \quad \frac{h_K^{1/2}}{\sqrt{\chi_K^*}} \|\llbracket \boldsymbol{\chi} \nabla \times \mathbf{E}_h \rrbracket \times \mathbf{n}_F\|_F \lesssim \left(1 + \left(k_{E,K} + \frac{c_{J,K}}{c_{E,K}} k_{P,K}\right) h_K\right) \|(\mathbf{E} - \mathbf{E}_h, \mathbf{J} - \mathbf{J}_h)\|_{\tilde{F}} \\ + \frac{h_K}{\sqrt{\chi_K^*}} \|\mathbf{r}_K\|_{\tilde{F}}$$

and hence (3.14) is a direct consequence of (3.16) and (3.17). \square

Lemma 3.9. *The estimate*

$$(3.18) \quad \eta_{\text{grad,div},K} \lesssim (1 + (k_{E,K} + k_{J,K}) h_K) \|(\mathbf{E} - \mathbf{E}_h, \mathbf{J} - \mathbf{J}_h)\|_{\tilde{K}} + \text{osc}_{\tilde{K}}$$

holds true for all $K \in \mathcal{T}_h$.

Proof. For a fixed $K \in \mathcal{T}_h$, let $\mathbf{r}_K := -\omega^2 \boldsymbol{\alpha} \mathbf{J}_h - \nabla(\zeta \nabla \cdot \mathbf{J}_h) - i\omega \mathbf{E}_h - i\omega \varrho_h \mathbf{K}_e$ and $\mathbf{r}_K^h := \varrho_h \mathbf{r}_K$. Then, after integrating by parts and thanks to (2.8a), we have that

$$\begin{aligned} \|\mathbf{r}_K^h\|_K^2 &\lesssim |(\mathbf{r}_K^h, b_K \mathbf{r}_K^h)_K| \\ &= |(\omega^2 \boldsymbol{\alpha}(\mathbf{J} - \mathbf{J}_h), b_K \mathbf{r}_K^h)_K + (\zeta \nabla \cdot (\mathbf{J} - \mathbf{J}_h), \nabla \cdot (b_K \mathbf{r}_K^h))_K + (i\omega(\mathbf{E} - \mathbf{E}_h), b_K \mathbf{r}_K^h)_K \\ &+ (i\omega(\mathbf{K}_e - \varrho_h \mathbf{K}_e), b_K \mathbf{r}_K^h)_K| \end{aligned}$$

and thus, using (2.8b), we obtain

$$\frac{h_K}{\sqrt{\zeta_K^*}} \|\mathbf{r}_K^h\|_K \lesssim \frac{\omega^2 h_K}{\sqrt{\zeta_K^*}} \|\boldsymbol{\alpha}(\mathbf{J} - \mathbf{J}_h)\|_K + \frac{h_K}{\sqrt{\zeta_K^*}} \|\zeta \nabla \cdot (\mathbf{J} - \mathbf{J}_h)\|_K + \frac{\omega h_K}{\sqrt{\zeta_K^*}} \|\mathbf{E} - \mathbf{E}_h\|_K + \text{osc}_K.$$

Recalling (2.4), we get that

$$(3.19) \quad \frac{h_K}{\sqrt{\zeta_K^*}} \|\mathbf{r}_K\|_K \lesssim (1 + (k_{J,K} + k_{P,K}) h_K) \|(\mathbf{E} - \mathbf{E}_h, \mathbf{J} - \mathbf{J}_h)\|_K + \text{osc}_K.$$

On the other hand, for $F \in \mathcal{F}_K$, we set $\mathbf{w}_F := b_F \mathcal{L}_F(\llbracket \zeta \nabla \cdot \mathbf{J}_h \rrbracket \mathbf{n}_F)$. Thanks to the fact that $\zeta \nabla \cdot \mathbf{J} \in H^1(\tilde{F})$ and $b_F \in H_0^1(\tilde{F})$, estimate (2.8a) and integration by parts reveal that

$$\|\llbracket \zeta \nabla \cdot \mathbf{J}_h \rrbracket\|_F^2 \lesssim |\langle \llbracket \zeta \nabla \cdot \mathbf{J}_h \rrbracket, \mathbf{w}_F \rangle_F| = |(\nabla(\zeta \nabla \cdot (\mathbf{J} - \mathbf{J}_h)), \mathbf{w}_F)_{\tilde{F}} + (\zeta \nabla \cdot (\mathbf{J} - \mathbf{J}_h), \nabla \cdot \mathbf{w}_F)_{\tilde{F}}|.$$

Using (2.1), we have that

$$\begin{aligned} \|\llbracket \zeta \nabla \cdot \mathbf{J}_h \rrbracket\|_F^2 &\lesssim \\ &| -(\omega^2 \boldsymbol{\alpha}(\mathbf{J} - \mathbf{J}_h), \mathbf{w}_F)_{\tilde{F}} + (\zeta \nabla \cdot (\mathbf{J} - \mathbf{J}_h), \nabla \cdot \mathbf{w}_F)_{\tilde{F}} - (i\omega(\mathbf{E} - \mathbf{E}_h), \mathbf{w}_F)_{\tilde{F}} + (\mathbf{r}_K^h, \mathbf{w}_F)_{\tilde{F}} | \end{aligned}$$

and using (2.8c)

$$\begin{aligned} \frac{h_K^{1/2}}{\sqrt{\zeta_K^*}} \|\llbracket \zeta \nabla \cdot \mathbf{J}_h \rrbracket\|_F &\lesssim \frac{\omega^2 h_K}{\sqrt{\zeta_K^*}} \|\alpha(\mathbf{J} - \mathbf{J}_h)\|_{\tilde{F}} + \frac{1}{\sqrt{\zeta_K^*}} \|\zeta \nabla \cdot (\mathbf{J} - \mathbf{J}_h)\|_{\tilde{F}} \\ &+ \frac{\omega h_K}{\sqrt{\zeta_K^*}} \|\mathbf{E} - \mathbf{E}_h\|_{\tilde{F}} + \frac{h_K}{\sqrt{\zeta_K^*}} \|\mathbf{r}_K\|_{\tilde{F}}. \end{aligned}$$

Then, (2.4) let us conclude that

$$(3.20) \quad \frac{h_K^{1/2}}{\sqrt{\zeta_K^*}} \|\llbracket \zeta \nabla \cdot \mathbf{J}_h \rrbracket\|_F \lesssim (1 + (k_{J,K} + k_{P,K})h_K) \|(\mathbf{E} - \mathbf{E}_h, \mathbf{J} - \mathbf{J}_h)\|_{\tilde{F}} + \frac{h_K}{\sqrt{\zeta_K^*}} \|\mathbf{r}_K\|_{\tilde{F}},$$

and (3.18) follows from (3.19) and (3.20). \square

Theorem 3.10. *The estimate*

$$(3.21) \quad \eta_K \lesssim \left(1 + \left(k_{E,K} + k_{J,K} + \left(1 + \frac{c_{J,K}}{c_{E,K}} \right) k_{P,K} \right) h_K \right) \|(\mathbf{E} - \mathbf{E}_h, \mathbf{J} - \mathbf{J}_h)\|_{\tilde{K}} + \text{osc}_{\mathcal{T}_{K,h}}$$

holds true for all $K \in \mathcal{T}_h$.

4. NUMERICAL EXAMPLES

4.1. Settings. We first present the settings and methodology common to our three examples.

4.1.1. Two-dimensional notations. Our numerical experiments are performed in a two-dimensional setting. We thus assume that the last component of the fields \mathbf{E} , \mathbf{J} , \mathbf{J}_e and \mathbf{K}_e vanishes and that the first two components only depend on the $(\mathbf{x}_1, \mathbf{x}_2)$ space variables. We further assume that the coefficients take the form

$$\boldsymbol{\varepsilon} = \begin{pmatrix} \varepsilon_{11} & \varepsilon_{12} & 0 \\ \varepsilon_{21} & \varepsilon_{22} & 0 \\ 0 & 0 & \varepsilon_{33} \end{pmatrix} \quad \boldsymbol{\chi} = \begin{pmatrix} \chi_{11} & \chi_{12} & 0 \\ \chi_{21} & \chi_{22} & 0 \\ 0 & 0 & \chi \end{pmatrix} \quad \boldsymbol{\alpha} = \begin{pmatrix} \alpha_{11} & \alpha_{12} & 0 \\ \alpha_{21} & \alpha_{22} & 0 \\ 0 & 0 & \alpha_{33} \end{pmatrix},$$

leading to

$$(4.1) \quad \begin{cases} -\omega^2 \boldsymbol{\varepsilon} \mathbf{E} + \mathbf{curl}(\chi \mathbf{curl} \mathbf{E}) + i\omega \mathbf{J} &= \mathbf{J}_e & \text{in } \Omega, \\ -\omega^2 \boldsymbol{\alpha} \mathbf{J} - \nabla(\zeta \nabla \cdot \mathbf{J}) - i\omega \mathbf{E} &= \mathbf{K}_e & \text{in } \Omega_m, \end{cases}$$

where the boldface notation now stands for two-components vectors and tensors. As usual, the two-dimensional curl operators are given by

$$\mathbf{curl} \phi = \partial_1 \phi_2 - \partial_2 \phi_1 \quad \mathbf{curl} \phi = (\partial_2 \phi, -\partial_1 \phi).$$

4.1.2. Perfectly matched layers. We employ perfectly matched layers to incorporate the radiation condition into a bounded computational domain. In our examples, we assume for the sake of simplicity that $\boldsymbol{\varepsilon}$ is diagonal and that the metallic particles are contained into a box $\Omega_0 := (-L, L)^2$ for some $L > 0$. We enclose Ω_0 into a larger box $\Omega := (-L - \ell, L + \ell)^2$ featuring an additional layer of size $\ell > 0$. Following [18], we define

$$d_j(\mathbf{x}) := 1 - \frac{3}{4} i \mathbf{1}_{|\mathbf{x}_j| > L}$$

for $j = 1$ or 2 , and construct modified coefficients

$$\tilde{\boldsymbol{\varepsilon}} := \begin{pmatrix} d_2/d_1 & 0 \\ 0 & d_1/d_2 \end{pmatrix} \boldsymbol{\varepsilon} \quad \tilde{\chi} = \frac{\chi}{d_1 d_2}.$$

These new coefficients are actually unchanged in Ω_0 , but take artificial values in the additional layer designed to absorb incoming radiations without spurious reflections. In the remaining of this section, we employ the artificial coefficients $\tilde{\varepsilon}$ and $\tilde{\chi}$, but omit the $\tilde{\cdot}$ notation to ease the presentation.

4.1.3. *Incident field injection.* We consider the scattering of an incident plane wave by metallic nanostructures. The total field \mathbf{E}^t splits into the (known) incident field \mathbf{E}^i and the scattered field \mathbf{E} that we numerically approximate. We decompose the computational domain as $\Omega = \Omega_m \cup \Omega_0 \cup \Omega_p$, where Ω_m corresponds to the metallic inclusions, Ω_p is the PML region, and $\Omega_0 := \Omega \setminus \overline{\Omega_m} \cup \overline{\Omega_p}$. \mathbf{E}^i is a solution to Maxwell's equations in Ω_0 . \mathbf{E} is a scattered field that satisfies the PML equation inside Ω_p . Finally, the total field \mathbf{E}^t satisfies the Maxwell-Drude system in $\Omega_0 \cup \Omega_m$. It follows that the pair (\mathbf{E}, \mathbf{J}) is solution to (4.1) with $\mathbf{J}_e := \mathbf{o}$ and $\mathbf{K}_e := i\omega\mathbf{E}^i$. In the forthcoming examples, we will only consider right-hand sides of this form, where

$$\mathbf{E}^i(\mathbf{x}) = \mathbf{p}e^{-ik\mathbf{d}\cdot\mathbf{x}},$$

where \mathbf{p}, \mathbf{d} are two unit vectors such that $\mathbf{p} \cdot \mathbf{x}$ and $k := \omega/c_0$. \mathbf{p} and \mathbf{d} respectively describe the polarization and the direction of the incident wave, while $c_0 := \sqrt{\varepsilon_0\mu_0}$ is the speed of light and k , the wavenumber.

4.1.4. *Coefficients.* The permittivity and permeability are set to the vacuum values in Ω_0 , that is

$$\varepsilon = \mathbf{I}\varepsilon_0, \quad \chi = \frac{1}{\mu_0},$$

with the aforementioned modification in the PML region Ω_p . In the metal, the coefficients α and ζ are defined from ω_p, γ and ϑ_F by

$$\alpha := \frac{1}{\omega_p^2\varepsilon_0} \left(1 - \frac{\gamma}{i\omega}\right) \mathbf{I}, \quad \zeta := \frac{3}{5} \frac{\vartheta_F^2}{\omega_p^2\varepsilon_0}.$$

The actual values of ω_p, γ and ϑ_F depend on the particular metal under consideration. For gold, we have

$$\omega_p := 1.390 \cdot 10^{16} \text{ rad} \cdot \text{s}^{-1}, \quad \gamma := 3.230 \cdot 10^{13} \text{ rad} \cdot \text{s}^{-1}, \quad \vartheta_F := 1.084 \cdot 10^6 \text{ m} \cdot \text{s}^{-1},$$

while for silver, we employ

$$\omega_p := 1.339 \cdot 10^{16} \text{ rad} \cdot \text{s}^{-1}, \quad \gamma := 1.143 \cdot 10^{14} \text{ rad} \cdot \text{s}^{-1}, \quad \vartheta_F := 1.465 \cdot 10^6 \text{ m} \cdot \text{s}^{-1}.$$

4.1.5. *Adaptive algorithm.* In the following examples, we employ the estimator described before to steer an adaptive mesh algorithm process. We fix once and for all the polynomial degree p and start with an initial mesh $\mathcal{T}_h^{(0)}$. Then, assuming we arrived at a mesh $\mathcal{T}_h^{(\ell)}$, we solve the finite element system associated with this mesh, and compute the associated elementwise error estimators η_K . These estimators are in turn use to output a new mesh $\mathcal{T}_h^{(\ell+1)}$, enabling the start of new iteration. We employ the software packages MUMPS [3] to solve the linear systems, and MMG [8] to generate the meshes. Algorithm 1 describes the resulting procedure. Notice that MMG refines an existing mesh \mathcal{T} by following new local mesh sizes \mathbf{h}_a that are given on the vertices \mathbf{a} of \mathcal{T} . As a result, Algorithm 1 includes a “translation” between the “element-based” estimator η_K and the data \mathbf{h}_a passed to MMG.

The adaptive procedure takes two additional parameters θ and ρ that controls how many elements are refined at each iteration, and how much their sizes is reduced. In the examples below, we always select $\theta := 0.05$ and $\rho := 0.5$. While we mean that we refine elements

Algorithm 1 Adaptive loop

```

1: procedure GENERATE_MESH( $\mathcal{T}, \mathbf{h}$ )
2:   generate  $\tilde{\mathcal{T}}$  by calling MMG with the input mesh  $\mathcal{T}$  and the vertex mesh size  $\mathbf{h}$ 
3:   return  $\tilde{\mathcal{T}}$ 
4: procedure GENERATE_MESH_SIZES( $\mathcal{T}, \eta, \theta, \rho$ )
5:   Let  $n_v$  denote the number of vertices of  $\mathcal{T}$ 
6:   zero initialize arrays  $\boldsymbol{\eta}$  and  $\mathbf{h}$  of size  $n_v$ 
7:   for each mesh element  $K \in \mathcal{T}$  do
8:     for each element vertex  $\mathbf{a} \in \mathcal{V}_K$  do
9:        $\boldsymbol{\eta}[\mathbf{a}] = \boldsymbol{\eta}[\mathbf{a}] + \eta_K$ 
10:       $\mathbf{h}[\mathbf{a}] = \max(\mathbf{h}[\mathbf{a}], h_K)$ 
11:   sort the vertices in an array ord such that  $\boldsymbol{\eta}[\text{ord}[j]]$  is non-decreasing
12:   find the smallest integer  $n \in \{1, \dots, n_v\}$  such that  $\sum_{j=1}^n \boldsymbol{\eta}[\text{ord}[j]]^2 \geq \theta \sum_{\mathbf{a}} \boldsymbol{\eta}[\mathbf{a}]^2$ .
13:   for  $j = 1, \dots, n$  do
14:      $\mathbf{h}[\text{ord}[j]] = \rho \mathbf{h}[\text{ord}[j]]$ 
15:   return  $\mathbf{h}$ 
16: procedure ADAPTIVE_LOOP( $\mathcal{T}^{(0)}, \ell_{\max}, \theta, \rho$ )
17:   for  $\ell = 0, \dots, \ell_{\max}$  do
18:     assemble the finite-element matrix associated with  $\mathcal{T}^{(0)}$ 
19:     solve the linear system with MUMPS
20:     compute the estimator  $\eta$ 
21:     compute the new mesh sizes  $\mathbf{h} = \text{GENERATE\_MESH\_SIZES}(\mathcal{T}^{(\ell)}, \eta, \theta, \rho)$ 
22:     generate the new mesh  $\mathcal{T}^{(\ell+1)} = \text{GENERATE\_MESH}(\mathcal{T}^{(\ell)}, \mathbf{h})$ 

```

that contribute to 5% of the total squared error, and that these elements have their diameter divided by two.

4.1.6. *Error measurements.* The analytical solutions for the examples below are not available, which complicates the numerical validation of the proposed error estimator. For a given mesh and polynomial p , if $(\mathbf{E}_h, \mathbf{J}_h)$ denotes the computed discrete solution, we compute a “reference” solution $(\tilde{\mathbf{E}}_h, \tilde{\mathbf{J}}_h)$ on the same mesh with $\tilde{p} = p+2$. We then employ the quantities

$$\xi_K := \left\| (\tilde{\mathbf{E}}_h - \mathbf{E}_h, \tilde{\mathbf{J}}_h - \mathbf{J}_h) \right\|_K \quad \xi^2 := \sum_{K \in \mathcal{T}_h} \xi_K^2$$

to obtain a measure of the discretization error.

4.1.7. *Comparison with uniform meshes.* We also benchmark the adaptive process against uniform meshes. To this end, we build for each geometry of interest a sequence of uniform meshes with MMG by simply requiring a maximal allowed mesh size. The mesh size is chosen so that the resulting number of degrees of freedom is similar to the structured meshes produced by the adaptive algorithm. This enables to quantify the accuracy improvement due to local refinements, since roughly the same computational cost is then required for the structured and the unstructured meshes. To avoid any confusion, we employ below the notation ξ_u and η_u for the error and estimator computed with the uniform meshes, while the quantities ξ_a and η_a relate to the adaptive meshes.

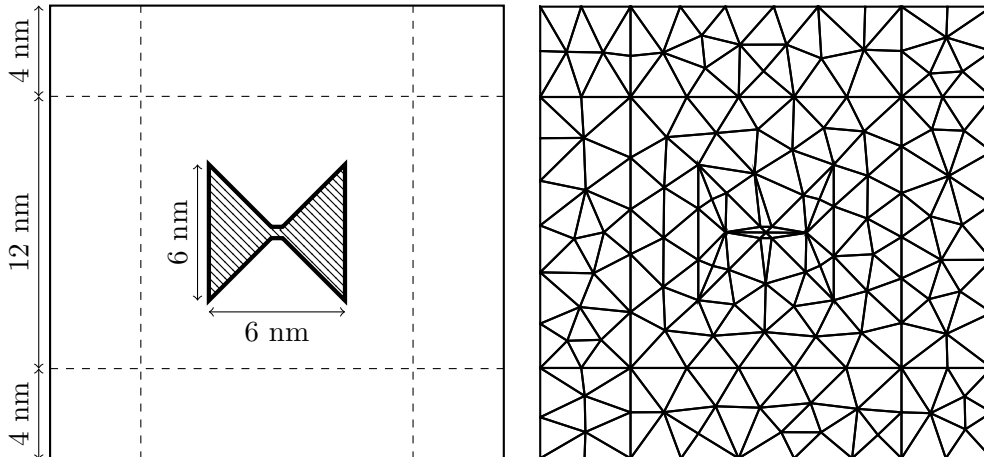


FIGURE 1. Settings of the bowtie example (right) and initial mesh for the adaptive algorithm (left).

4.2. Gold bowtie antenna. Our first example is a bowtie nano-antenna made of gold, as depicted on Figure 1. The incidence angle is $\theta = \pi/3$, and thus $\mathbf{d} = (\cos \theta, \sin \theta)$ and $\mathbf{p} = (-\sin \theta, \cos \theta)$. We consider three frequencies, namely $\omega = 0.8\omega_P$, $0.9\omega_P$ and ω_P . Figure 2 presents the reference solution computed on the finest mesh. The case where $\omega = \omega_P$ is of particular interest: it can be seen on Figure 2 that the desired light-focusing effect is effectively achieved.

We start the adaptive loop with the initial mesh on the right panel of Figure 1 and run this loop for 80 iterations with the polynomial degree $p = 1$. Figure 3 depicts the behaviour of the errors ξ_a and ξ_u plotted against the number of degrees of freedom N_{dofs} . The accuracy is significantly improved on adaptive meshes for a similar number of degrees of freedom. Besides, we observe the optimal convergence rate in $N_{\text{dofs}}^{-(p+1)/2}$, which means that the estimator correctly steers the mesh refinement process. Figure 4 shows the effectivity index of the estimator for both adaptive and uniform meshes. The effectivity index first oscillates before stabilizing asymptotically for fine meshes. This behaviour is typical of non-coercive problems [6]. It is also in agreement with efficiency estimate (3.21) of Theorem 3.10 which states that the estimator may become inefficient on coarse meshes. Finally, we present the elementwise actual error distribution and the estimator η_K in the central region of the mesh for $\omega = 0.8\omega_P$ in Figure 5. While the scales of the left and right panels are different, the (relative) agreement between the actual error and the estimator is excellent.

4.3. Silver nanotip. Here, we model the silver nanotip depicted on the left panel of Figure 6. We consider three frequencies of interest, namely $\omega := 0.7\omega_P$, ω_P and $1.3\omega_P$. In every case, we select an incident planewave with direction $\mathbf{d} = (1, 0)$, and polarization $\mathbf{p} = (0, 1)$, and we begin the adaptive algorithm on the initial mesh represented in the right panel of Figure 6. The discrete solution is computed with a polynomial degree $p = 2$ and we run the adaptive loop for 50 iterations. The reference solutions computed on the finest meshes are presented in Figure 7.

Figure 8 shows the convergence history for adaptive and uniform meshes. The adaptive meshes drastically improve the accuracy, and yield the optimal convergence rate $N_{\text{dofs}}^{-(p+1)/2}$.

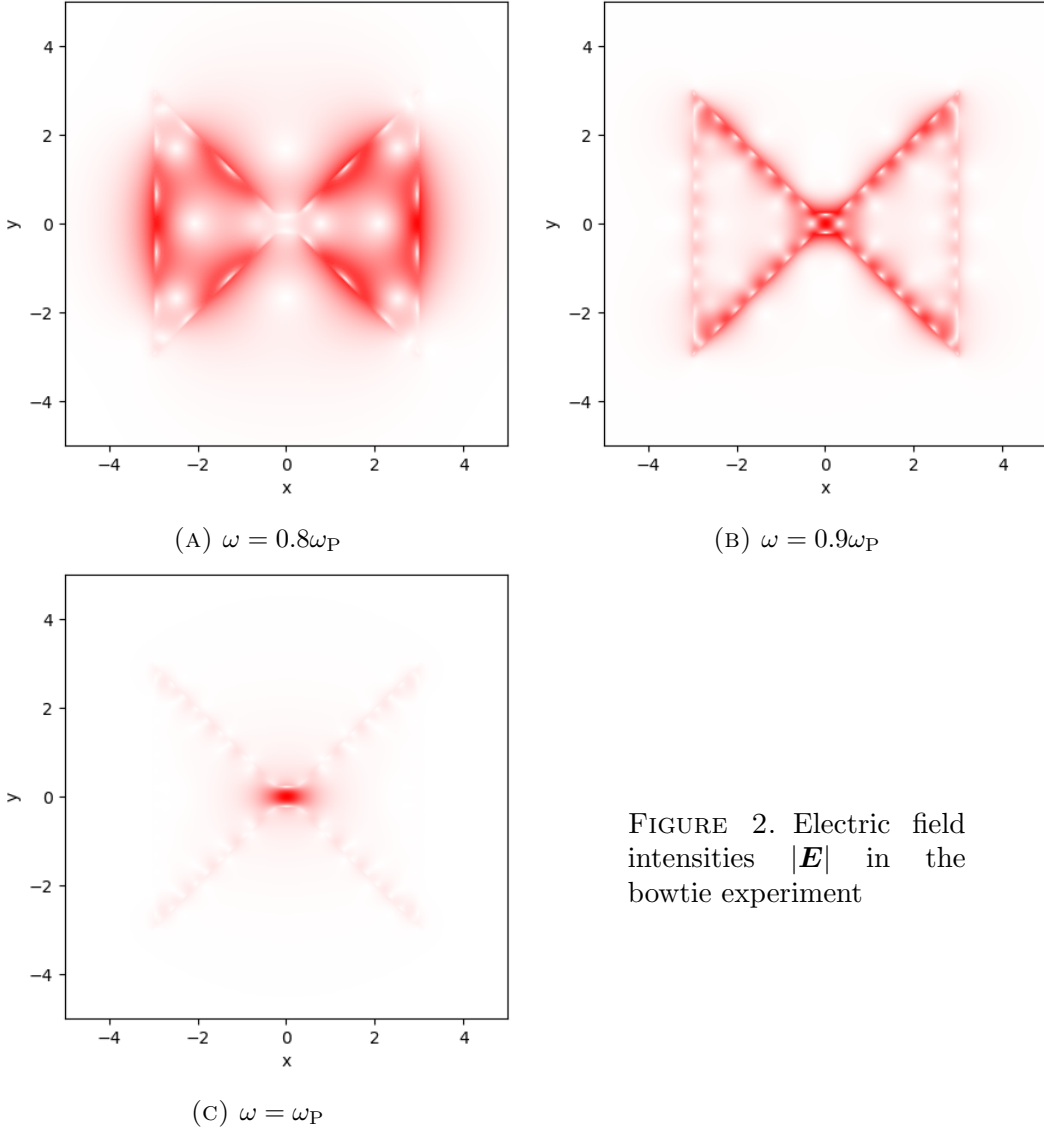


FIGURE 2. Electric field intensities $|\mathbf{E}|$ in the bowtie experiment

The case where $\omega = 0.7\omega_P$ is particularly instructive, since uniform meshes clearly converge suboptimally. We present the effectivity indices in Figure 9. As previously stated, we observe a usual behaviour, which is in agreement with previous works and our key theoretical results. In Figure 10, we represent the elementwise error distribution and the estimator in a neighborhood of the nanotip at iteration #25 of the adaptive algorithm. We observe a nice agreement between the estimator and the actual error for the selected frequencies. Finally, Figure 11 features the final mesh produced by the adaptive algorithm at the last iteration (#50). The meshes are finer close to the inclusion, with specific refinements close to the edges and corners of the tip, as to be expected.

4.4. Gold V-groove channel. The last example is a “V-groove” channel depicted in Figure 12. The incidence angle is again $\theta = \pi/3$, with $\mathbf{d} = (\cos\theta, \sin\theta)$ and $\mathbf{p} = (-\sin\theta, \cos\theta)$. The reference solutions produced on the finest meshes are presented

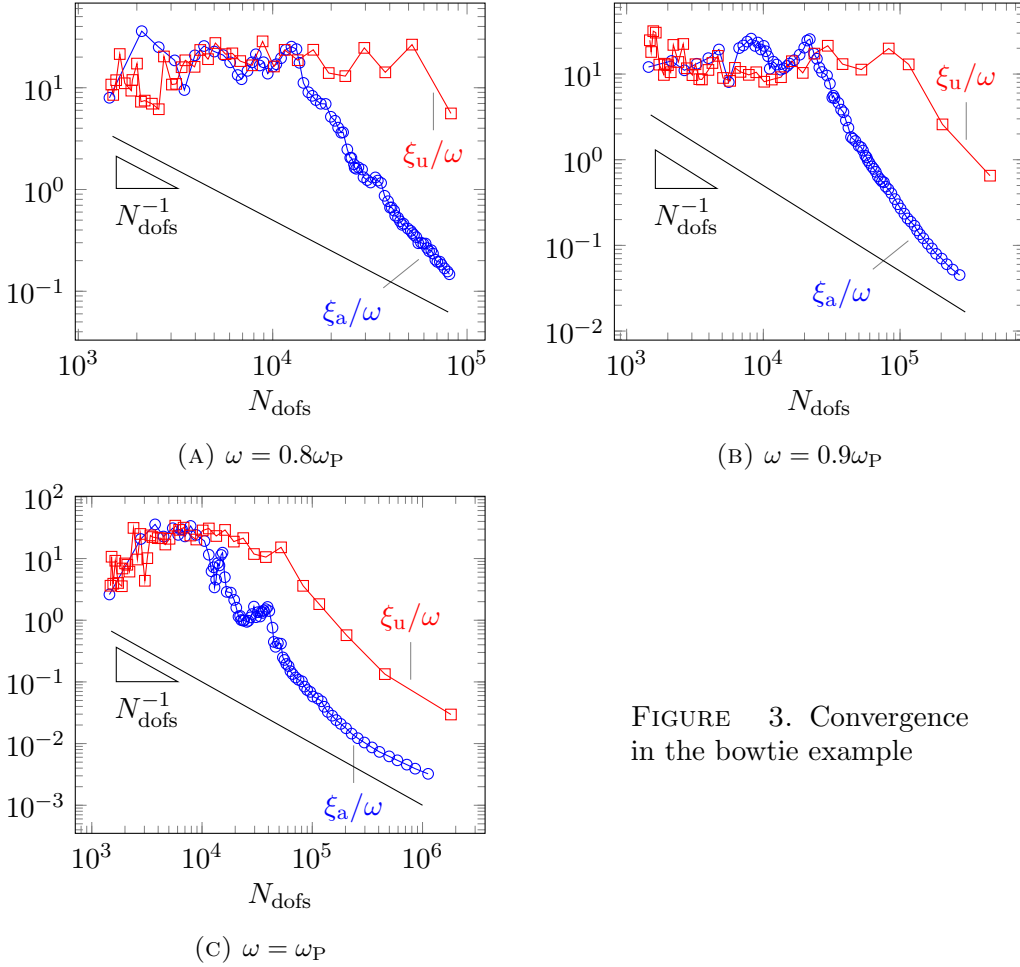


FIGURE 3. Convergence in the bowtie example

in Figure 13 for $\omega = 0.8\omega_P$, $0.9\omega_P$ and ω_P . The desired behaviour is observed in the case $\omega = 0.9\omega_P$ where the electric field is localized in the “V” cavity, which can be used to design a waveguide along the transverse direction. We run the adaptive loop for 50 iterations starting with the initial mesh of Figure 12 and $p = 3$.

As in the other experiments, Figure 14 presents the behaviour of the actual error against the number of degrees of freedom, and we observe a large accuracy enhancement on adaptive meshes, together with an optimal convergence rate. The effectivity indices are represented on Figure 15. They exhibit a nicer behaviour than in the previous experiments. This is linked to the fact that a higher polynomial degree is employed with similar starting mesh sizes, which shorten the “pre-asymptotic regime” where the reliability constant may depend on the mesh size. Figure 16 shows the actual and estimated error distributions are very similar, again illustrating the quality of the proposed estimator.

5. CONCLUSION

We propose a novel residual-based *a posteriori* error estimator for finite element discretizations of Maxwell’s equations coupled with a non-local hydrodynamic Drude model taking into account spatial dispersion effects in metallic nanostructures. At the theoretical level, we

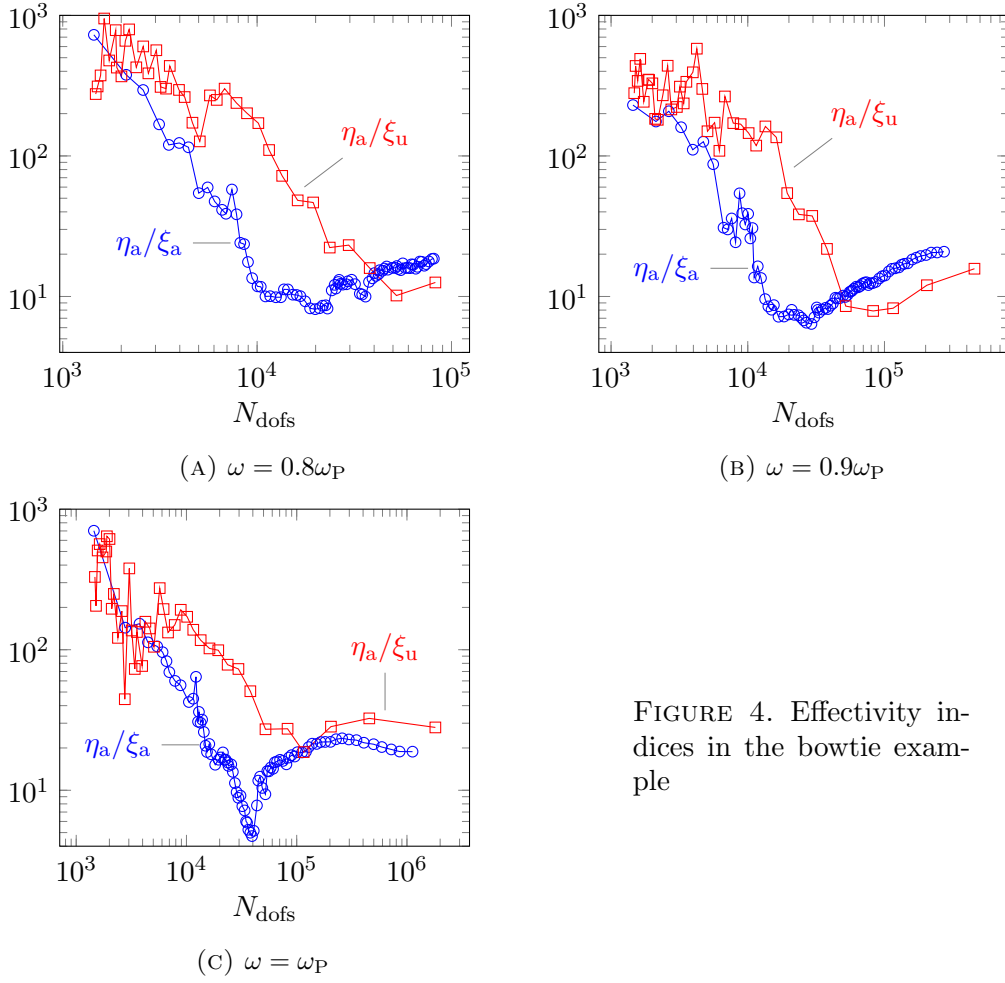


FIGURE 4. Effectivity indices in the bowtie example

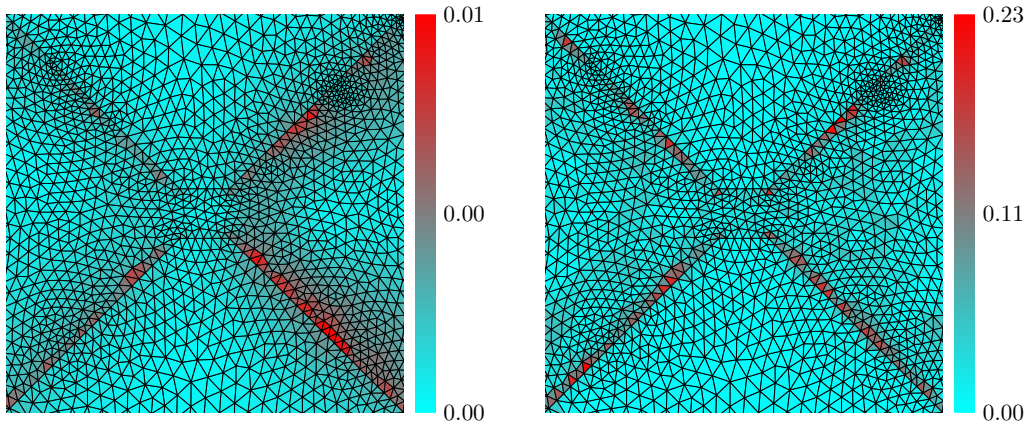


FIGURE 5. Actual (left panel) and estimated (right panel) errors at the iteration #80 of the adaptive algorithm for the bowtie antenna example with $\omega = 0.8\omega_P$.

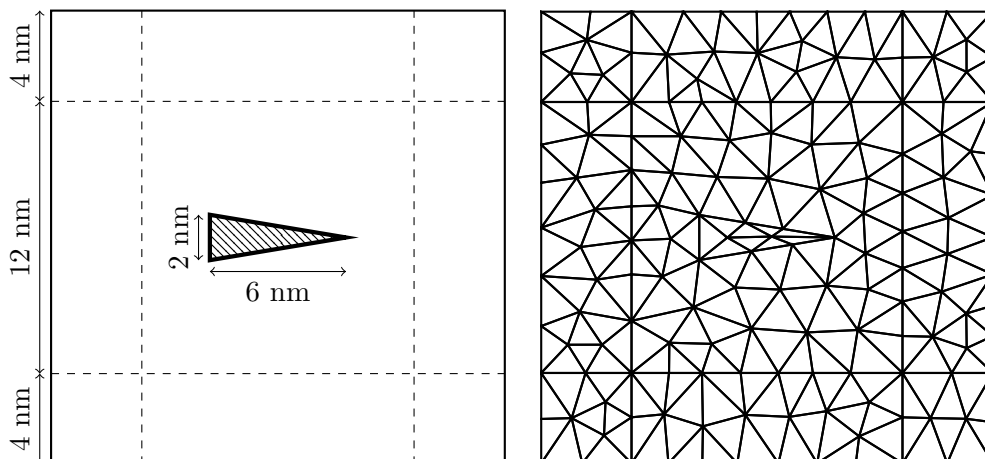


FIGURE 6. Settings of the nanotip example (right) and initial mesh for the adaptive algorithm (left).

establish reliability and efficiency of the estimator. We also propose a number of relevant two-dimensional examples where the error estimator drives an adaptive procedure. We observe the expected optimal convergence rate meaning that the estimator correctly steers the adaptive process. Besides, the adaptive algorithm enables substantial computational savings, as compared to the use of uniform meshes. These preliminary results are very promising, and future work will focus on more realistic three-dimensional benchmarks.

REFERENCES

1. R. Adams and J. Fournier, *Sobolev spaces*, Academic Press, 2003.
2. M. Ainsworth and J. T. Oden, *A posteriori error estimation in finite element analysis*, Wiley, 2000.
3. P. R. Amestoy, I. S. Duff, and J. Y. L'Excellent, *Multifrontal parallel distributed symmetric and unsymmetric solvers*, *Comput. Methods Appl. Mech. Engrg.* **184** (2000), 501–520.
4. R. Beck, R. Hiptmair, R. H. W. Hoppe, and B. Wohlmuth, *Residual based a posteriori error estimators for eddy current computation*, *ESAIM Math. Model. Numer. Anal.* **34** (2000), 159–182.
5. M. L. Brongersma, *Plasmonic photodetectors, photovoltaics, and hot-electron devices*, *Proc. IEEE* **104** (2016), 2349–2361.
6. T. Chaumont-Frelet and P. Vega, *Frequency-explicit a posteriori error estimates for finite element discretizations of Maxwell's equations*, submitted, preprint hal-02943386, 2020.
7. P. G. Ciarlet, *The finite element method for elliptic problems*, SIAM, 2002.
8. C. Dobrzynski, *MMG3D: User guide*, Tech. Report 422, Inria, 2012.
9. P. Drude, *Zur elektronentheorie der metalle*, *Ann. Phys.* **306** (1900), 566–613.
10. H. Duan, A. I. Fernández-Domínguez, M. Bosman, S. A. Maier, and J. K. W. Yang, *Nanoplasmonics: classical down to the nanometer scale*, *Nano Lett.* **12** (2012), 1683–1689.
11. A. Ern and J.L. Guermond, *Finite element quasi-interpolation and best approximation*, *ESAIM Math. Model. Numer. Anal.* **51** (2017), 1367–1385.
12. V. Girault and P. A. Raviart, *Finite element methods for Navier-Stokes equations: theory and algorithms*, Springer-Verlag, 1986.
13. R. Hiptmair and C. Pechstein, *Regular decompositions of vector fields - continuous, discrete and structure-preserving*, Tech. Report 2019-18, ETH seminar for applied mathematics, 2019.
14. K. R. Hiremath, L. Zschiedrich, and F. Schmidt, *Numerical solution of nonlocal hydrodynamic drude model for arbitrary shaped nano-plasmonic structures using nédélec finite elements*, *J. Comput. Phys.* **321** (2012), 5890–5896.

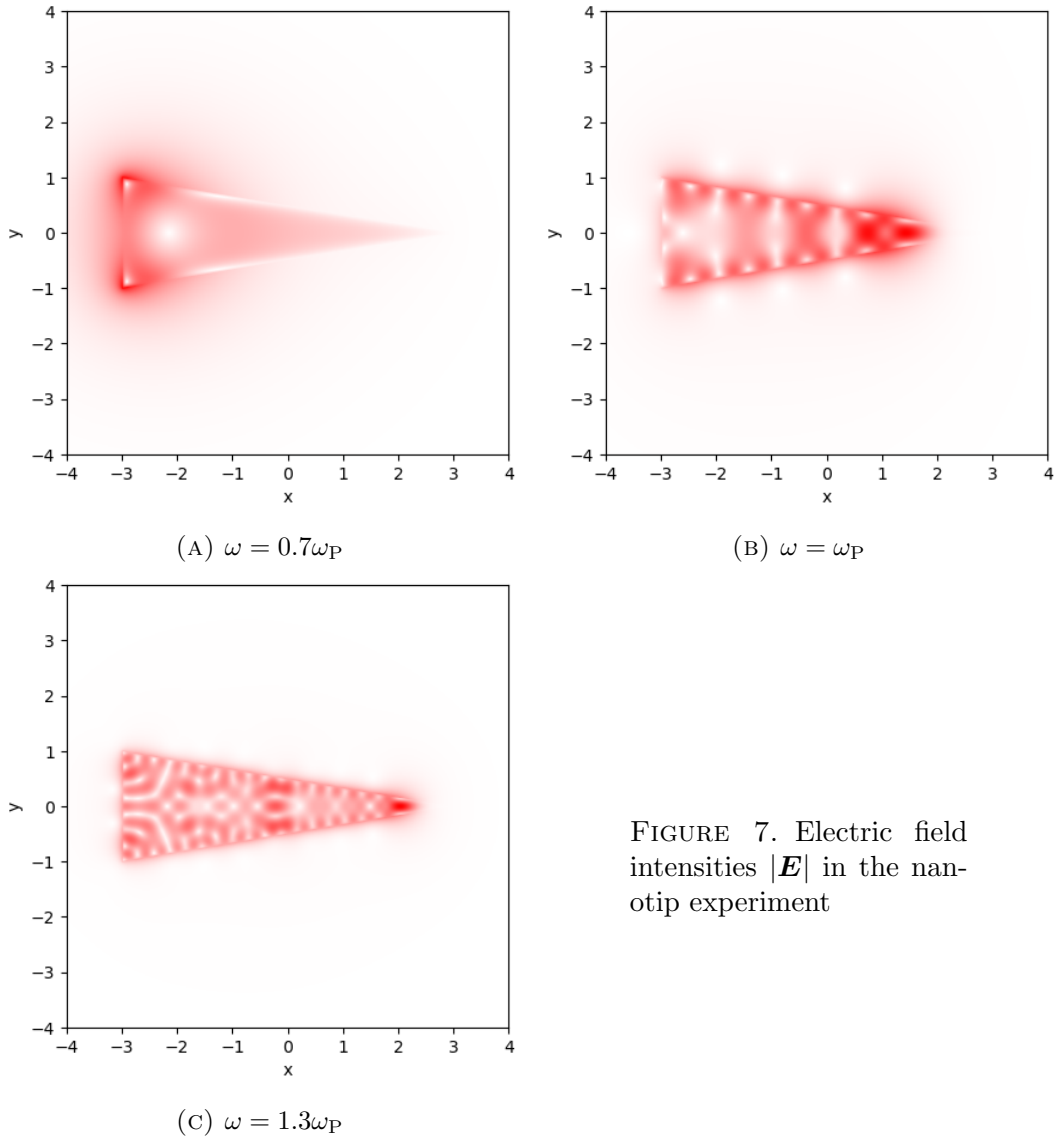


FIGURE 7. Electric field intensities $|\mathbf{E}|$ in the nanotip experiment

15. L. Li, S. Lanteri, N. A. Mortensen, and M. Wubs, *A hybridizable discontinuous Galerkin method for solving nonlocal optical response models*, *Comput. Phys. Comm.* **19** (2017), 99–107.
16. C. Ma, Y. Zhang, and J. Zou, *Mathematical and numerical analysis of a nonlocal Drude model in nanoplasmonics*, submitted, preprint arXiv:1906.04790 [math.NA], 2019.
17. S. A. Maier, *Plasmonics: fundamentals and applications*, Springer, 2007.
18. P. Monk, *Finite element methods for Maxwell's equations*, Oxford science publications, 2003.
19. S. Nicaise and E. Creusé, *A posteriori error estimation for the heterogeneous Maxwell equations on isotropic and anisotropic meshes*, *Calcolo* **40** (2003), 249–271.
20. L. Novotny and N. Van Hulst, *Antennas for light*, *Nat. Photonics* **5** (2011), 83–90.
21. R. F. Oulton, V. J. Sorger, D. A. Genov, D. F. P. Pile, and X. Zhang, *A hybrid plasmonic waveguide for subwavelength confinement and long-range propagation*, *Nat. Photonics* **2** (2008), 496–500.
22. S. Raza, S. I. Bozhevolnyi, M. Wubs, and N. A. Mortensen, *Nonlocal optical response in metallic nanostructures*, *J. Phys. Condens. Matter* **27** (2015), 183204.

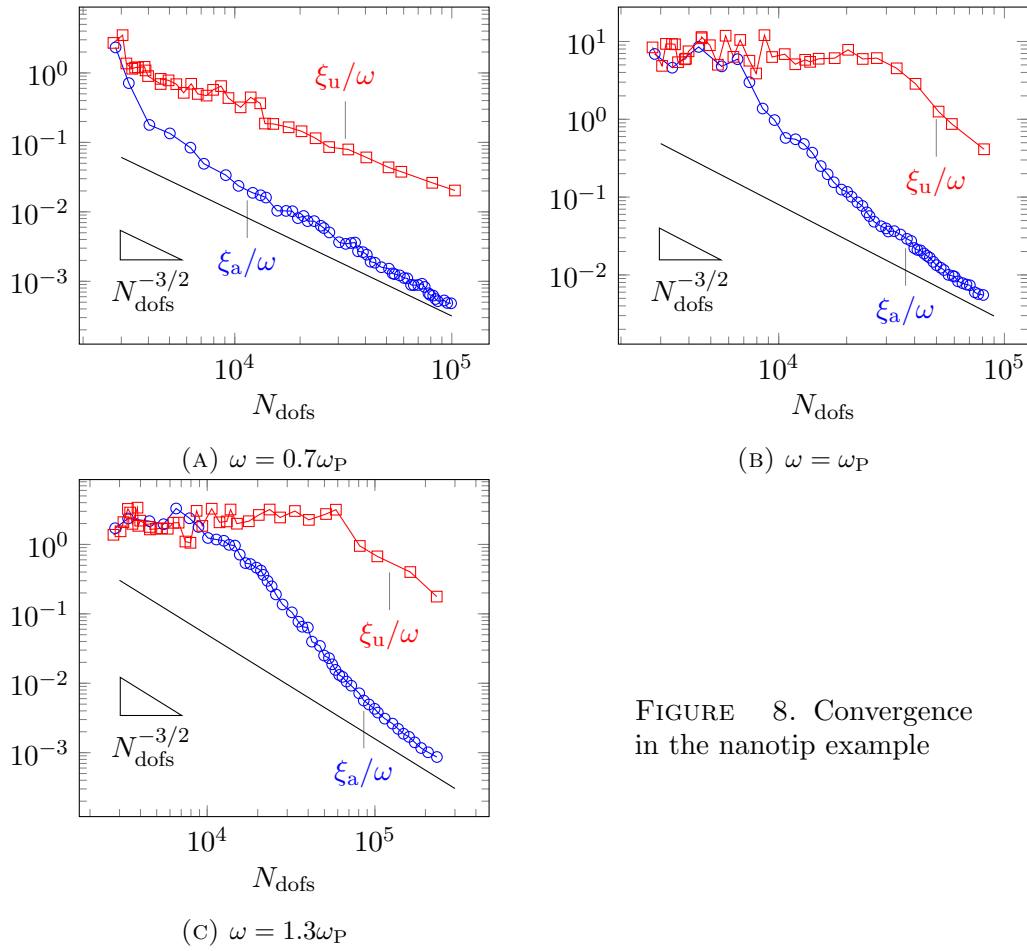


FIGURE 8. Convergence in the nanotip example

23. J. S. Smalley, F. Vallini, Q. Gu, and Y. Fainman, *Amplification and lasing of plasmonic modes*, Proc. IEEE **104** (2016), 2323–2337.
24. M. E. Stewart, C. R. Anderton, L. B. Thompson, J. Maria, S. K. Gray, J. A. Rogers, and R. G. Nuzzo, *Nanostructured plasmonic sensors*, Chem. Rev. **108** (2008), 494–521.
25. G. Toscano, S. Raza, A.-P. Jauho, N. A. Mortensen, and M. Wubs, *Modified field enhancement and extinction by plasmonic nanowire dimers due to nonlocal response*, Opt. Express **20** (2012), 4176–4188.
26. R. Verfürth, *A posteriori error estimation and adaptive mesh-refinement techniques*, J. Comput. Appl. Math. **50** (1994), 67–83.
27. F. Vidal-Codina, N. C. Nguyen, S.-H. Oh, and J. Peraire, *A hybridizable discontinuous Galerkin method for computing nonlocal electromagnetic effects in three-dimensional metallic nanostructures*, J. Comput. Phys. **355** (2018), 548–565.
28. X. Z. Zheng, M. Kupresak, R. Mittra, and G. A. E. Vandenbosch, *A boundary integral equation scheme for simulating the nonlocal hydrodynamic response of metallic antennas at deep-nanometer scales*, IEEE Trans. Antennas Propag. **66** (2018), 4759–4771.

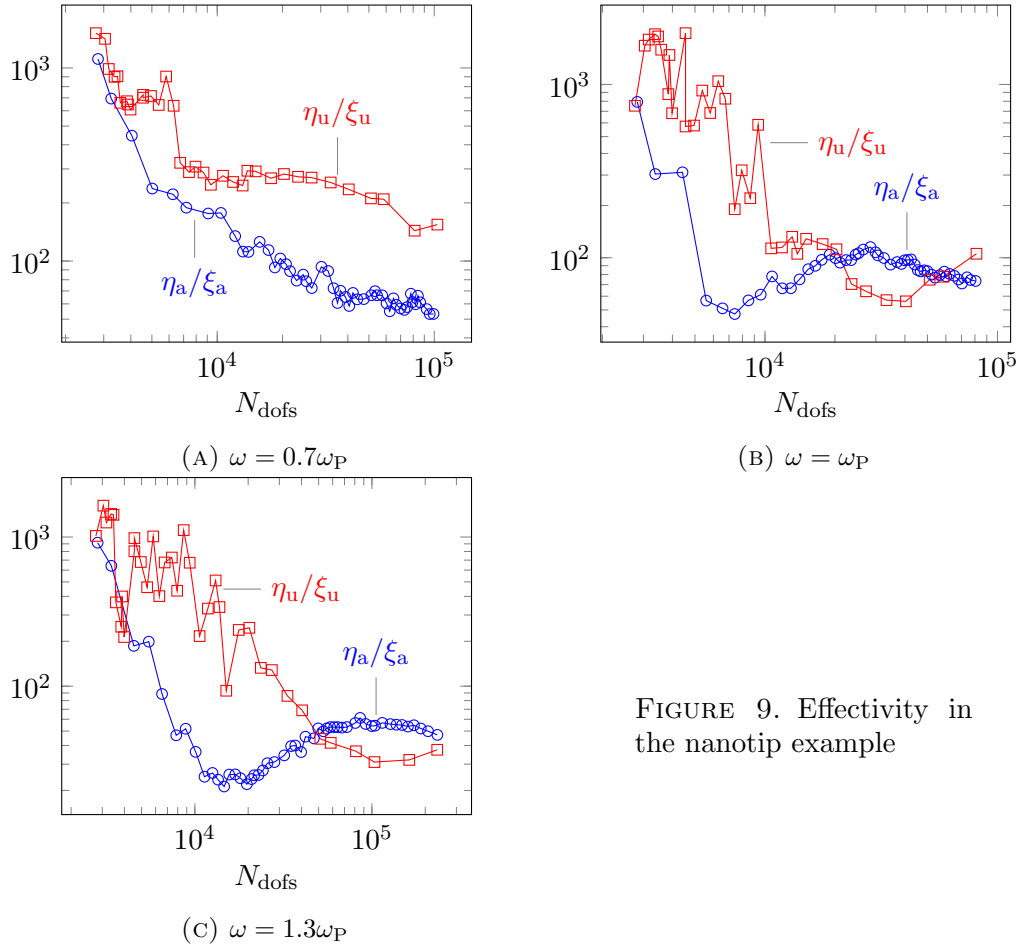


FIGURE 9. Effectivity in the nanotip example

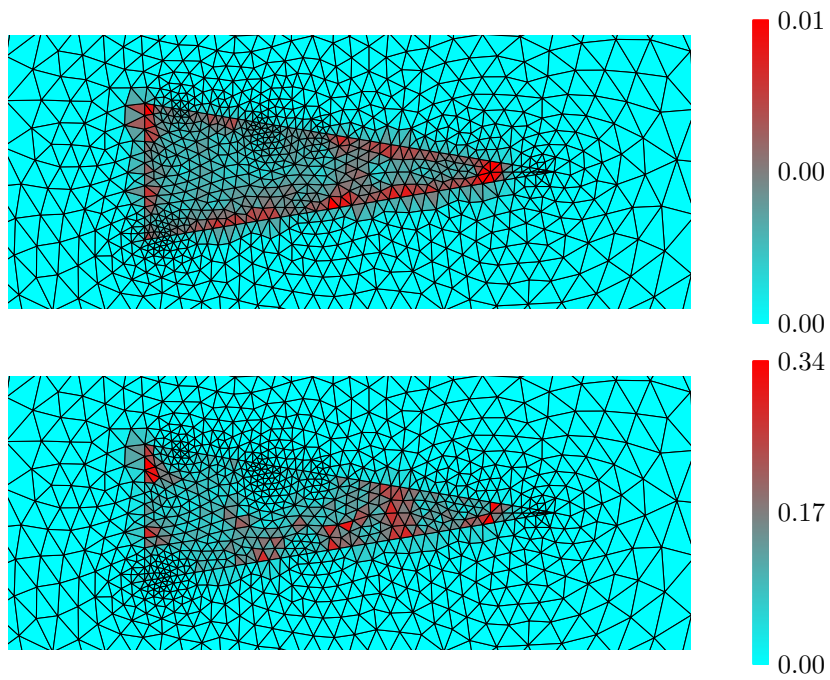


FIGURE 10. Actual (top panel) and estimated (bottom panel) errors at the iteration #25 of the adaptive algorithm for the nanotip example with $\omega = 1.3\omega_p$.

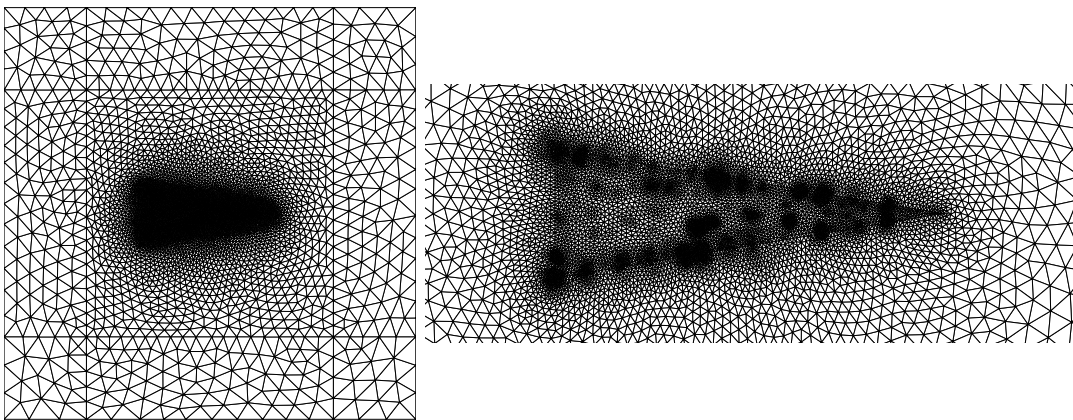


FIGURE 11. Computational mesh at the #50 iteration of the adaptive algorithm for the nanotip example with $\omega = 1.3\omega_p$. The right panel presents a focus on the inclusion.

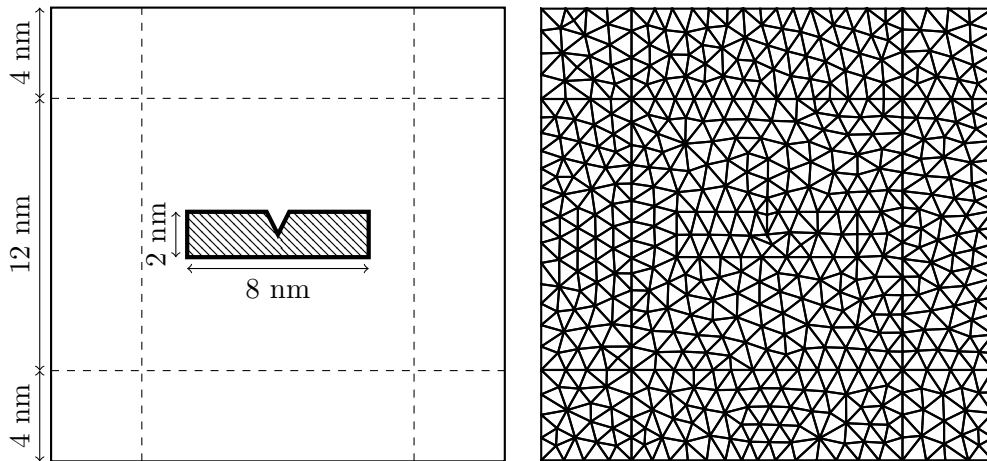


FIGURE 12. Settings of the V-groove example (right) and initial mesh for the adaptive algorithm (left).

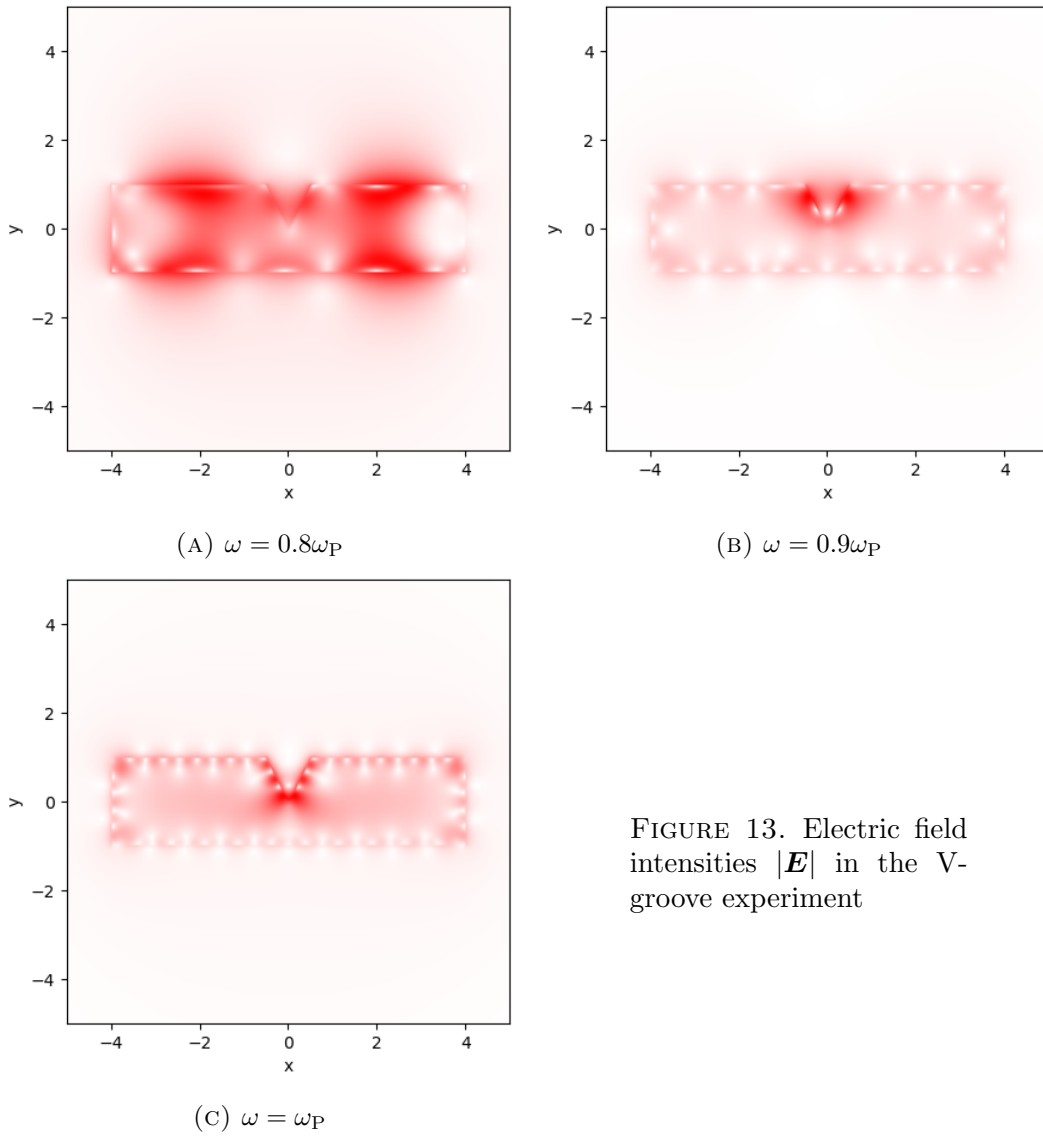


FIGURE 13. Electric field intensities $|\mathbf{E}|$ in the V-groove experiment

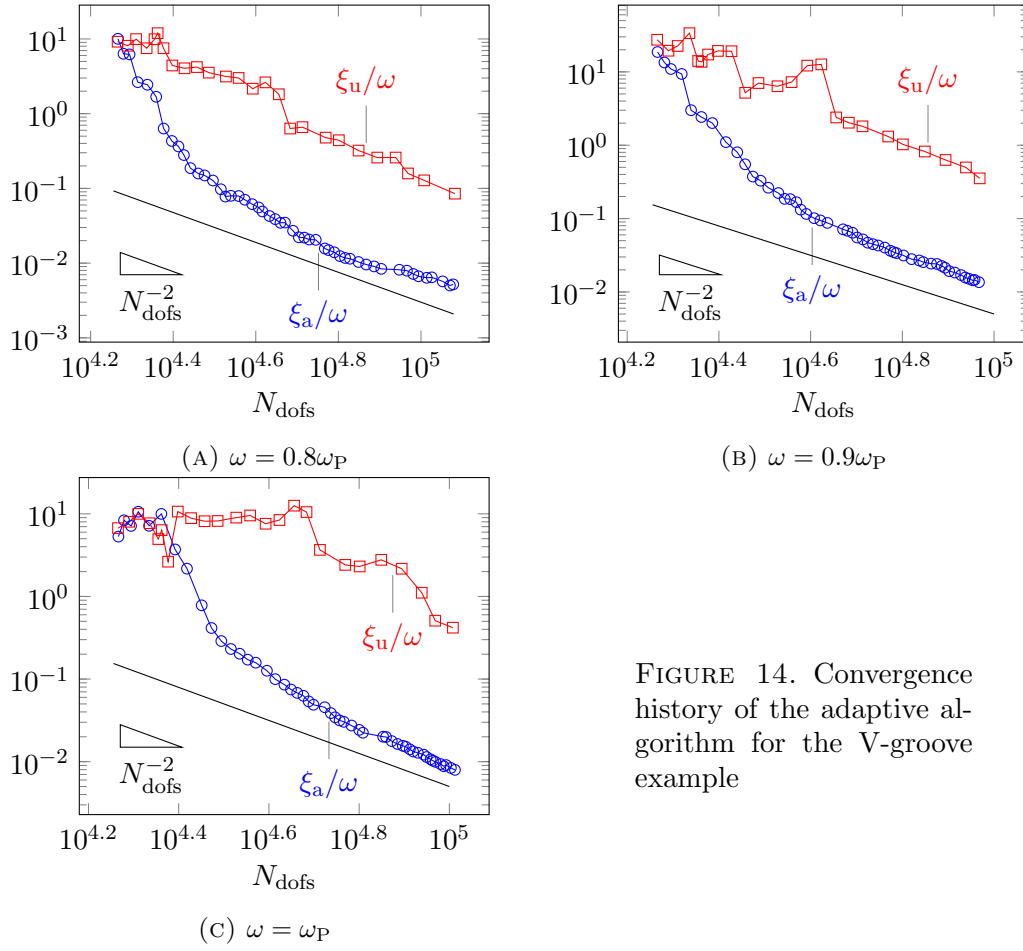
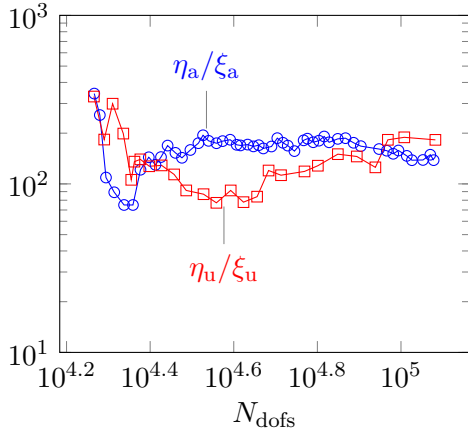
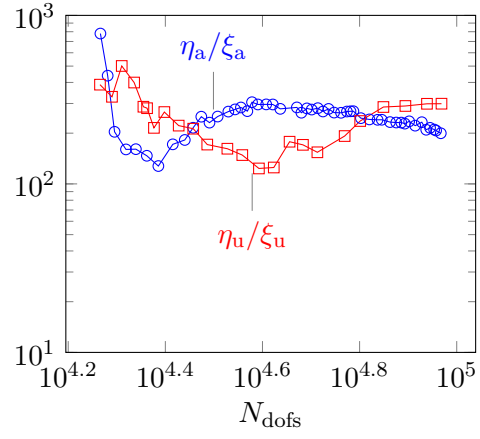


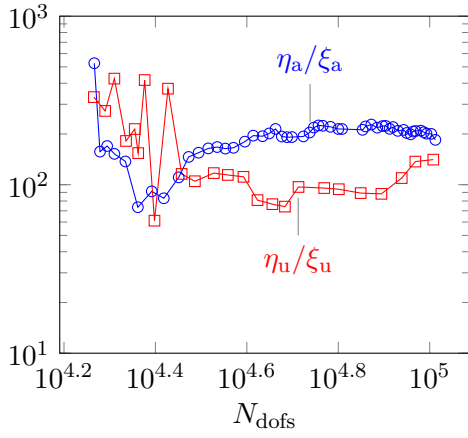
FIGURE 14. Convergence history of the adaptive algorithm for the V-groove example



(A) $\omega = 0.8\omega_P$



(B) $\omega = 0.9\omega_P$



(C) $\omega = \omega_P$

FIGURE 15. Convergence history of the adaptive algorithm for the V-groove example

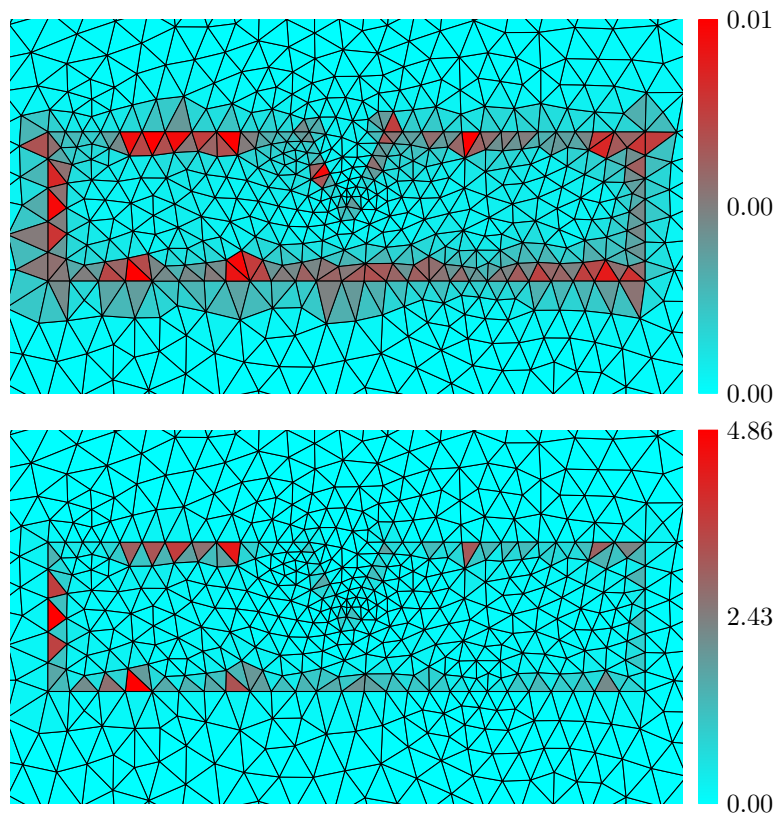


FIGURE 16. Actual (top panel) and estimated (bottom panel) errors at the iteration #80 of the adaptive algorithm for the V-groove example with $\omega = 0.9\omega_p$.